International Journal of Disaster Risk Reduction 137 (2026) 106085

Contents lists available at ScienceDirect

International Journal of Disaster Risk Reduction

journal homepage: www.elsevier.com/locate/ijdrr

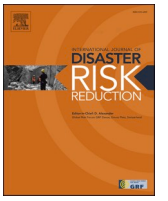

# A probabilistic performance-based framework for heat vulnerability and risk assessment of buildings

Simona Bianchi [a,*], Jonathan Ciurlanti [b]

[a] Delft University of Technology, 2628 BL, Delft, the Netherlands
[b] Arup, 1043 CA, Amsterdam, the Netherlands

ARTICLE INFO

*Keywords:*
Climate resilience
Heat vulnerability
Performance-based
Risk assessment
Uncertainty

ABSTRACT

As climate-induced hazards increase rapidly, the built environment's limited preparedness highlights the urgent need to enhance resilience. Although risk assessment frameworks inform resilient design decisions for many hazards, heat stress at the building scale are often addressed using simplified code-based approaches. Emerging heat fragility models provide a basis for risk quantification; however, a unified heat risk framework that estimates multi-domain consequences (social, economic, environmental) accounting for multi-factor uncertainties (climate, building, occupant) is still lacking. To address this gap, this paper proposes a probabilistic method grounded in performance-based engineering principles. The approach integrates hazard analysis, building performance evaluation, fragility modeling and loss estimation, and employs a Monte Carlo framework to propagate uncertainty across all stages. Its step-by-step implementation is demonstrated on a multi-story building under varying design conditions and climate scenarios, proving the framework's ability to quantify probable maximum losses and incorporate them into risk matrices. The case study results show energy demand and carbon costs increasing by around 13% under high-warming scenarios, with heat-related mortality nearly tripling in naturally ventilated conditions, enabling building-level comparison across performance thresholds and hazard severities. Probabilistic loss functions translate these impacts into expected annual losses, further highlighting the importance of passive survivability, as cost and carbon metrics are projected to increase by 50% while mortality risk rises sharply for the analyzed building. These annualized losses can inform building-level design decisions and multi-hazard resilience planning, as the proposed approach aligns with probabilistic models and risk metrics used in catastrophe modeling to compare natural and climate hazards.

## 1. Introduction

The building sector plays a central role in climate change mitigation and adaptation, functioning both as a major contributor to energy use and emissions and as the primary protection layer against extreme heat. Buildings account for 30% of global energy consumption and 26% of energy-related emissions (8% direct, 18% indirect from electricity and heat production) [1]. Beyond emissions, building design directly shapes the urban thermal environment: HVAC systems release substantial waste heat into the outdoors, building mass alters thermal inertia and diurnal temperature cycles, and façade radiative properties govern surface

* Corresponding author.Delft University of Technology, 2628 BL, Delft, the Netherlands.
*E-mail address:* s.bianchi@tudelft.nl (S. Bianchi).

https://doi.org/10.1016/j.ijdrr.2026.106085
Received 17 September 2025; Received in revised form 27 February 2026; Accepted 3 March 2026
Available online 4 March 2026

temperatures and radiative heat exchange [2]. At the same time, buildings determine most of the heat exposure people experience. Characteristics such as access to air conditioning, insulation levels, airtightness, shading and ventilation capacity are strongly linked to heat-related morbidity and mortality [3]. As economic barriers and power outages can limit the use of air conditioning during extreme events, building design must prioritize passive survivability, thus the ability to maintain safe indoor conditions without mechanical cooling. This moves the design focus beyond efficiency toward ensuring thermal safety during extreme heat events, a pressing need as heatwaves escalate in frequency and severity and urban heat islands raise ambient temperatures in already vulnerable areas. These trends are driving higher cooling demand and electricity use, creating a feedback loop of rising emissions. Although countries are committing to decarbonizing the electrical grid, the International Energy Agency projects a 25-30% increase in electricity demand by 2030 [4], with peak summer loads posing rising risks to grid reliability. Meanwhile, climate change is expected to increase heat-related mortality: under current policies consistent with ~3 °C of warming, Europe could face roughly 54,974 additional temperature-related deaths annually by 2100, with ageing populations particularly at risk [5].

Understanding how buildings perform under a warming climate is therefore critical. This requires performance metrics that go beyond traditional energy efficiency to include indoor thermal safety, passive survivability and the building's interaction with the surrounding urban environment. Consequently, mitigation and adaptation strategies must evaluate multiple performance dimensions (thermal resilience, energy demand, waste-heat emissions) alongside downstream consequences such as financial losses, carbon emissions and health impacts. Multi-domain performance-based assessments indicate that even new energy code-compliant buildings can exhibit significant vulnerabilities to extreme heat, and highlight both synergies and trade-offs among performance objectives e.g. Refs[2,6] For example, highly insulated buildings can reduce energy demand but may retain excess heat overnight if ventilation is inadequate. Similarly, holistic solutions, such as green buildings e.g. Refs [7,8] can provide multiple co-benefits, including reducing overall losses, mitigating global warming, lowering local temperatures and enhancing urban heat adaptation. These studies highlight the need for assessment approaches that consider heat stress and evaluate holistic performance, rather than relying solely on single-metric optimization.

In addition to adopting multi-performance approaches, there is a growing demand for more reliable building performance assessments. This has driven the increasing adoption of uncertainty quantification and probabilistic modeling to enhance prediction reliability and support more informed building design. Uncertainty in building energy simulations arises from diverse sources and is commonly classified into aleatory uncertainty, reflecting inherent natural variability, and epistemic uncertainty, which stems from limited data or incomplete knowledge. In the context of heat stress, uncertainty arises from hazard modelling (e.g., future climate), building attributes (e.g., thermal properties, occupancy), and the reliability of the model (e.g., assumptions, completeness). Climate projections themselves are inherently uncertain and quickly become outdated, emphasizing the need to use multiple climate models for reliable forecasting [9]. Among all sources, occupant behavior, such as the use of appliances and windows, has the greatest impact on energy demand and introduces the most significant uncertainty in building energy models [10]. Climate change can indirectly influence these behaviors, highlighting the need to assess their role in energy adaptation and consider behavior-based interventions as a key climate strategy. Local effects also shape probabilistic assessments, including variations in energy service demand (e.g., heating, cooling) and differences among building groups by sector (e.g., residential, commercial) or location (e.g., city, region) [11].

These uncertainties can be incorporated into probabilistic analyses to evaluate the range of possible building performance outcomes. Approaches, as those proposed by Sun et al. [12] and Scarpa et al. [13], demonstrate how such methods can improve predictions of energy-use intensity and total utility costs by employing Monte Carlo simulation and sensitivity analysis, which account for random errors and variability across key physical, financial and time-dependent parameters. These approaches have been successfully applied to quantify and compare the performance of energy efficient retrofit strategies (e.g., Refs. [14,15]). Beyond energy efficiency, probabilistic analysis has been applied to assess thermal comfort in buildings, capturing uncertainties associated with occupant behavior, presence and activity patterns (e.g., Refs. [16,17]). Recent studies have also proposed uncertainty-based frameworks in the context of climate change and building energy simulations at scale (e.g., Refs. [13,18,19]). These approaches have demonstrated improvements in the accuracy of average demand load profiles compared to deterministic archetype-based simulations, particularly with respect to estimating energy needs and peak loads. Although probabilistic assessments in the field are gaining interest, existing models are primarily used to define ranges of energy-related outcomes and are not integrated into full risk frameworks that quantify broader consequences. In particular, environmental and social impacts remain underexplored [20], despite becoming increasingly critical in the context of heat stress.

In decision-making frameworks, risk is commonly defined as a combination of hazard, vulnerability and exposure. For heat stress, the hazard reflects the probability of a specific extreme event. Vulnerability describes a building or system's susceptibility to fail or perform inadequately under heat stress, shaped by its physical characteristics and design quality. Exposure represents the value of elements at risk, such as occupants or critical systems. The growing need for a multi-dimensional framework that integrates such components to assess urban heat risks is well recognized [21]. Recent research has increasingly focused on the assessment of urban heat vulnerability, reflecting the growing urgency of mitigating overheating and its adverse impacts on human health. In particular, studies have investigated the role of building-specific factors, such as indoor overheating, access to air conditioning and building age, in shaping heat vulnerability, developing new vulnerability indices (e.g., Refs. [20,22]) and more representative physiological metrics to capture cumulative and consecutive exposure to hazardous thermal conditions [23]. In parallel, probabilistic models have been proposed to generate more robust outputs for planning and operational decision-making. These models quantify heat impacts in terms of e.g. the probability of average annual heat-related mortality, probabilistic overheating curves describing residential discomfort and probabilistic energy demand estimation (e.g., Refs. [24–27]). However, they typically focus on large-scale probabilistic modelling using historical data/statistics and often do not account for building-level uncertainties (such as envelope properties or cooling set-points) that influence the risk reduction of individual asset strategies. Other studies have instead adopted engineering-based

approaches, developing fragility functions that quantify the probability of exceeding thermal or energy-related thresholds as heat intensity increases (e.g., Refs. [28,29]). However, methods for incorporating fragility functions into probabilistic heat risk modelling within a catastrophe-modelling framework remain limited, leaving unresolved how such functions can be used to quantify risk metrics (expected annual loss).

Addressing this gap would enable the integration of heat vulnerability with physical vulnerability within a unified framework for building-level risk assessment. For example, recent studies have explored such combinations using heat and seismic fragility models or total economic losses e.g., Refs[30,31] providing guidance for integrated seismic and energy-efficient building interventions. In this case, to support a truly multi-risk analysis, a framework analogous to that used in seismic risk assessment should be developed, following the principles of Performance-Based Earthquake Engineering (PBEE) [32–34]. PBEE is a performance-based decision-support framework designed to link hazard, building performance and decision-making. Performance simulation and probabilistic modeling are components within the PBEE framework, which enhances decision-making by offering robust quantification of probable impacts (e.g., for earthquakes: repair costs, casualties, carbon emissions associated with reconstruction) while systematically accounting for all sources of uncertainty. Compared to typical risk frameworks designed for portfolio or regional level assessments using top-down statistical or historical loss data, PBEE provides detailed insights at the individual building level, enabling evaluation of design choices and asset-specific interventions. It identifies which hazard intensities, building characteristics and system failures lead to the exceedance of performance thresholds (resulting in expected loss) and supports diagnosis and targeted mitigation. This framework has already been extended to other hazards, such as flood and wind e.g. Refs.[35,36]. Applying the same approach to heat stress similarly enables uncertainty-informed consequence assessment. In line with approaches commonly used in catastrophe modeling, these consequences can be expressed either as Expected Annual Losses (EAL), derived from hazard curves across multiple return periods, or as probable maximum losses associated with specific hazard scenarios. This flexibility provides a structured basis for multi-hazard decision-making and resilience planning, where EAL commonly serve as the risk metric for comparing the impacts of natural and climate hazards.

To address this need, this study (i) develops a PBEE-based mathematical framework for heat risk modeling, using a Monte Carlo approach to propagate uncertainties and derive probabilistic estimates of key decision variables such as monetary loss, carbon emissions and loss of life; (ii) defines new performance-based design and/or risk matrices for heat hazard, to guide building design and retrofit decisions according to targeted levels of expected multi-domain consequences; and (iii) integrates heat fragility into a quantitative risk assessment approach, to estimate annualized losses (EAL) for use in multi-hazard risk models. To demonstrate its applicability, the framework is validated using a multi-story building under different design conditions (air conditioning, natural ventilation) and climate scenarios. This application illustrates how the step-by-step methodology enables heat risk quantification and how this information can support scenario comparison.

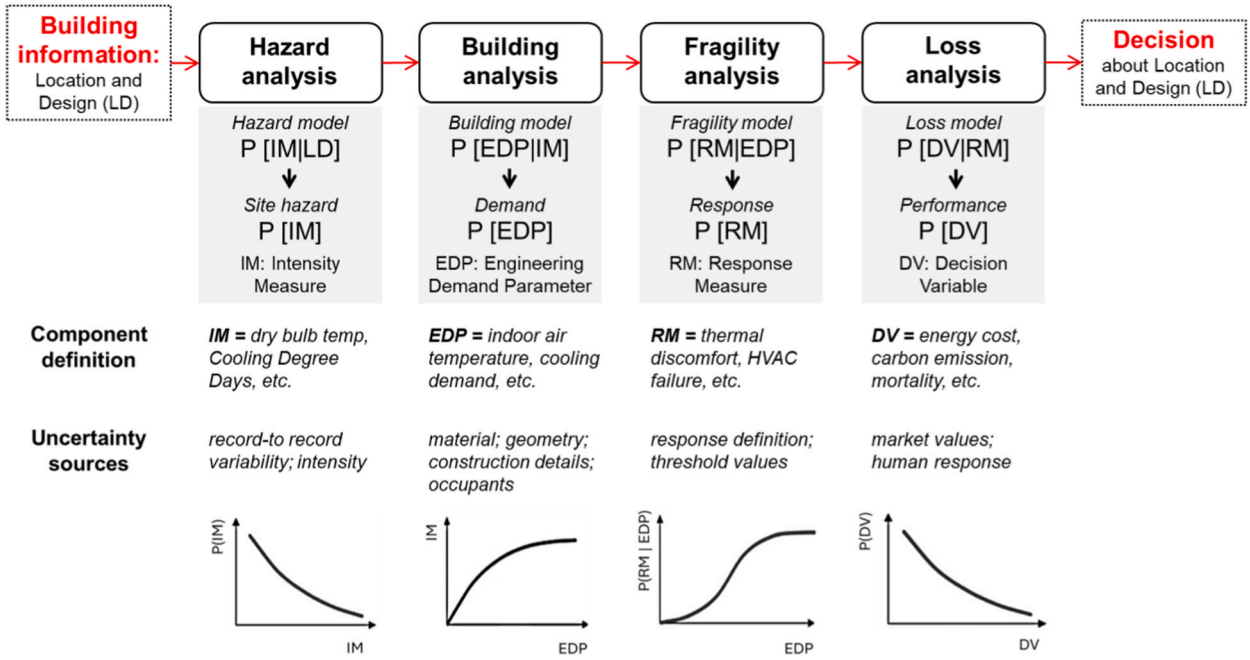


**Fig. 1.** Probabilistic framework for heat loss estimation.

## 2. Probabilistic framework for heat loss estimation

### 2.1. Framework formalization

As previously mentioned, the framework follows the structure of the PBEE methodology [32–34]. Accordingly, a probabilistic framework is established by integrating all key analysis components - hazard, building response, fragility, loss - each influenced by specific sources of uncertainty (Fig. 1). Hazard analysis involves defining the Intensity Measure (IM), i.e. modelling the weather and accounting for the uncertainty of its variables at a specific location (Section 2.1.1). Building analysis identifies the Engineering Demand Parameters (EDPs), and refers to the building's response to weather hazards, accounting for uncertainties related to material and geometric properties, construction details and occupant behavior (Section 2.1.2). Fragility analysis results in the definition of a Response Measure (RM), which characterizes the building's capacity while accounting for uncertainties in its definition and in the performance threshold levels (Section 2.1.3). In this framework, fragility curves are not based on physical building damage but on the building's response to heat, considering impacts on functionality and occupant well-being [28,29]. Loss analysis involves quantifying consequences (such as fatalities or loss of productivity) - referred to as Decision Variables (DVs) - that describe the building's vulnerability, accounting for variations in human response and economic factors such as market prices (Section 2.1.4). Defining the four components (IM, EDP, RM, DV) enables detailed component-based loss modelling of buildings, where vulnerabilities of elements, such as the envelope (façade), HVAC systems or sub-assemblies (thermal zones or rooms), are combined to quantify expected heat impacts.

Given the various sources of uncertainty, the analysis components (hazard, building, fragility, loss) cannot be defined by deterministic values, but rather by probability functions. As discussed below (Section 2.1.4), these functions can be combined using the total probability theorem, resulting in the probability of exceedance for various values of a DV over the building's lifecycle [32–34]. The process assumes Markovian independence, such that the conditional probabilities at each stage depend only on the outcome of the preceding stage. This structure allows domain experts to focus on their respective specialties while contributing to the overall assessment; for example, a climatologist can develop climate-informed hazard models, while an engineer can focus on analyzing the building's response. The approach is well suited for probabilistic heat-risk modelling because it provides a consistent modular framework that: (i) enables the explicit representation and propagation of multi-domain uncertainties; (ii) maintains a clear separation of analysis stages, allowing individual modules to be refined independently without requiring simultaneous consideration of the others; and (iii) ensures compatibility with other risk models (e.g. seismic, flood, wind), facilitating the integration of heat vulnerability with physical vulnerability.

The complete PBEE approach is valuable for rigorous analyses, as it allows propagation of component uncertainties, such as envelope properties or occupant behavior, to identify localized impacts in specific rooms or zones. This detailed representation supports prioritization of interventions within a building and enables more informed targeted decision-making, especially when complex assets are analyzed. For broader building-scale assessments, a simplified three-step approach is also proposed (Fig. 2). This approach defines fragility functions directly in terms of the IM, bypassing the use of EDPs functions. Although the EDP stage is not modelled explicitly, this is inherently captured within the building simulation. In this case, the model links the IM (e.g., dry bulb temperature) directly to performance outcomes (e.g., thermal discomfort), enabling efficient yet rigorous probabilistic vulnerability assessment. Furthermore, fragility modelling can be omitted when evaluating continuous operational or aggregate consequences (such as annual energy costs or operational carbon emissions) which can be probabilistically quantified based on continuous performance metrics rather than discrete degradation thresholds, as demonstrated in Section 3.3.2.

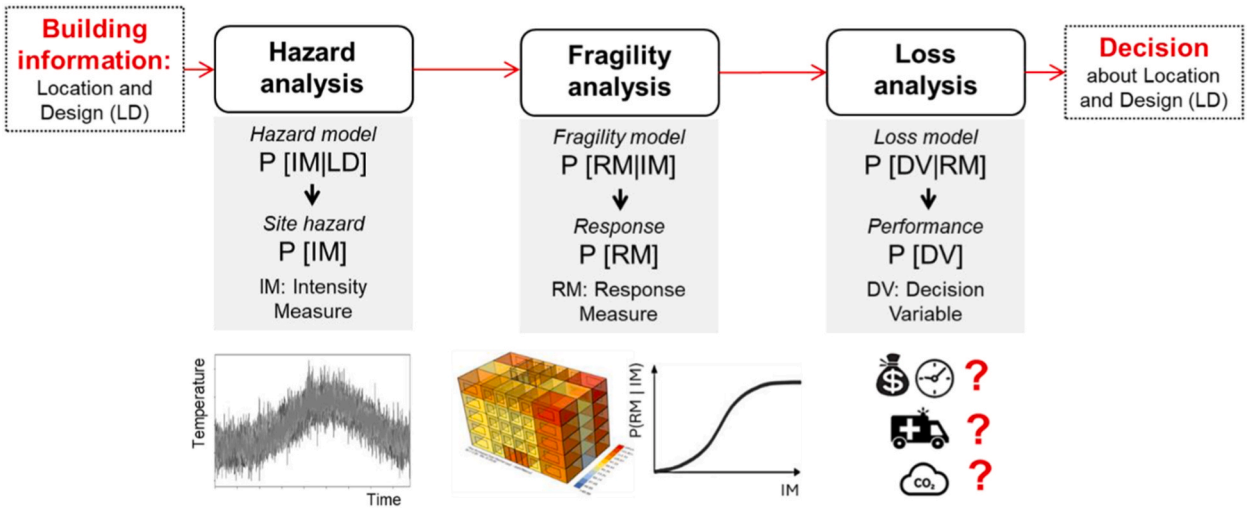


**Fig. 2.** Building-level probabilistic heat loss estimation.

### 2.1.1. Hazard analysis

Hazard analysis is conducted to characterize heat stress in a probabilistic framework. In this step, IMs are defined to quantify the severity of heat events. An IM represents a metric describing the hazard, such as extreme dry-bulb temperature or Heat Index (HI), which directly impacts building performance and occupant exposure. Hazard curves are then derived, showing the variation of a selected IM versus its Mean Annual Frequency (MAF) or annual frequency of exceedance, representing how often a given intensity is expected to occur. The choice of IM is linked to the building assets and functions it affects (for example, envelope thermal performance, cooling systems or indoor comfort) so that the hazard characterization is relevant to the probabilistic assessment of heat-related consequences.

Hazard analysis involves defining a set of weather data for the specific building location, requiring a sufficient number of weather values to generate meaningful statistical data for building analysis. These data include multiple variables (such as dry-bulb temperature, dew-point temperature, relative humidity, wind direction and speed, solar radiation) and can be obtained from historical records, where variability in these factors contributes to discrepancies in building simulation outcomes. The data can also be defined using climate projections, which are probabilistic in nature, as equally probable climate years can be generated to represent a single scenario, further contributing to variability in the hazard definition.

When focusing on current climate, historical data from weather stations can be used, with uncertainties arising from data sources, availability and the weather file generation process. For instance, Typical Meteorological Year (TMY) [37] is typically employed in simulations to account for inter-annual record variability (i.e. differences in year-to-year weather records) through condensing data from multiple sequential years into one characteristic weather file. When considering future weather, several uncertainties are also involved: climate model, emission scenario and downscaling technique. Future weather is generated using a global climate model at a large spatial resolution that captures large-scale circulation patterns, with spatial and temporal downscaling applied to reflect local climatic conditions and define hourly data [38]. Further uncertainties arise from the pathway scenarios, which are based on the expected rates of change in atmospheric concentrations and greenhouse gas emissions as defined by the Intergovernmental Panel on Climate Change, considering distinct socio-economic projections [39]. Each scenario includes projections for 30-year climatological averages centered around 2050, 2100 and 2150, and is linked to the time at which specific warming levels are expected to be reached, making it model-dependent.

Once the weather data is collected, hazard curves can be derived to express the annual frequency or probability of exceedance of the IM over a specific period (Fig. 3). An empirical cumulative distribution function can be first derived from the observed annual data over multiple years, calculating for each IM value how many data points are less or equal to that value and by dividing for the total number of data points (Eq. (1)):

$$P(IM \leq im) = \frac{n_{IM \leq im}}{N} \tag{1}$$

$P$ represents the cumulative probability, i.e., the probability that the IM is less than or equal to a given value $im$, based on the observed data. The exceedance probability is the complement of the cumulative distribution, and represents the probability that the intensity measure will exceed a given value $im$ in a given year. It is commonly referred to as the annual probability of exceedance for that IM (Eq. (2)).

$$P(IM > im) = 1 - P(IM \leq im) \tag{2}$$

By plotting the IM on the x-axis and the annual probability of exceedance on the y-axis, a hazard curve and the likelihood of exceeding different temperature thresholds can be derived. This exceedance probability can be used to derive the probability that an intensity measure ($IM$) will exceed a given value during a reference period of $N$ years, by assuming that all annual maxima are independent and considering the compounding effect of probabilities over multiple years (Eq. (3)):

$$P_N(IM > im) = 1 - (1 - P(IM > im))^N \tag{3}$$

Calculation of IMs falls within the realm of climatologists, and the selection of the most appropriate IM for probabilistic assessment

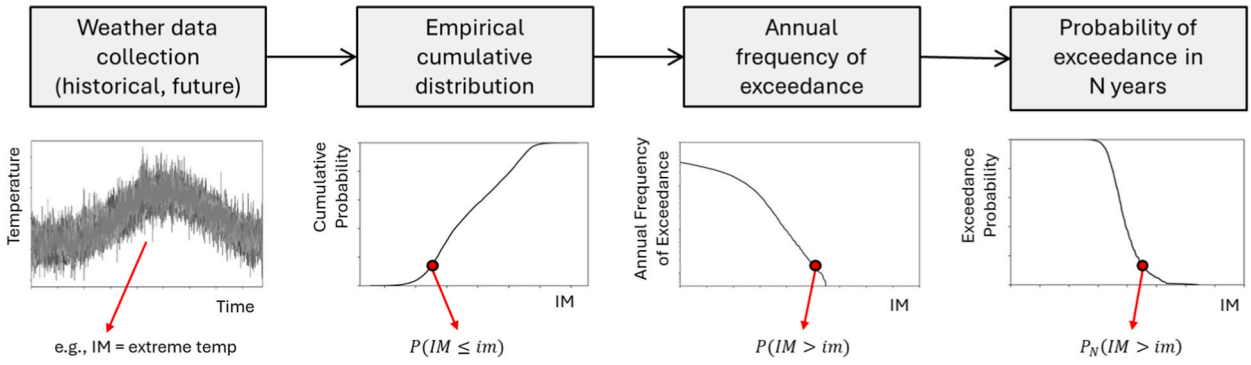


**Fig. 3.** Derivation of hazard curve.

should strike a balance between simplicity and accuracy, as this choice can influence the EDP vs IM distributions. Additionally, in urban environments, the Urban Heat Island (UHI) effect, i.e., the temperature difference between urban areas and surrounding rural areas [40], should be considered when defining hazard curves. This is crucial, as different urban zones can exhibit different hazard profiles.

### 2.1.2. Building analysis

Building energy simulations are conducted to probabilistically quantify the building response to heat hazards (Fig. 4). A numerical model of the building is developed, explicitly accounting for uncertainties in its definition that influence both indoor heat exposure and heat exchange with the surrounding environment. The main sources of uncertainty considered are.

- *Material properties*, particularly the thermal characteristics of the building envelope, which govern heat transfer, thermal inertia and radiative heat exchange. Uncertainty in thermal conductivity, density, specific heat capacity and thermal and solar absorptivity affects indoor overheating, surface temperatures and diurnal temperature dynamics.
- *Construction details*, including the composition and condition of opaque and glazed walls, roofs and floors. Variability in layer configuration influences thermal resistance and airtightness, while material ageing or deterioration can alter heat gains and ventilation effectiveness.
- *Occupant behavior*, encompassing daily occupancy patterns and the use of equipment, ventilation and air-conditioning systems. These behaviors introduce uncertainty in internal heat gains, cooling demand and waste heat rejection to the outdoor environment, which in turn affects both indoor exposure and local thermal conditions.
- *Design variations*, such as access to air conditioning, cooling set-point temperatures, shading strategies and ventilation capacity. These parameters directly influence occupants' heat exposure and are strongly associated with heat-related health outcomes, while also affecting building energy use during extreme heat events.

An additional source of modelling uncertainty arises from the quality of the building definition, particularly with respect to geometric properties. For existing buildings, this uncertainty is linked to the completeness and reliability of available documentation (e.g. architectural drawings describing the as-built condition) and the extent of field investigations conducted to verify construction details. For new buildings, uncertainty reflects assumptions regarding construction quality control and the degree to which the completed building matches the design intent.

For each hazard intensity level, building energy simulations estimate responses using selected EDPs, defined by the performance target and analysis focus (e.g., energy demand, overheating), with peak EDP values computed. Different weather files are generated to represent various IMs, using historical or future climate data derived through techniques such as morphing [41], stochastic weather generators [42] or dynamical downscaling of climate models [43]. These weather files serve as inputs to building simulation tools (e.g., EnergyPlus [44]), enabling the estimation of building responses and the generation of a wide range of EDPs. A random sampling technique can be then used to propagate the input uncertainty to the output and draw a range of possible occurrences, with the number of data points for each of the selected EDPs at an intensity level (IM = $im$) equal to the number of analyses conducted for that intensity level multiplied by the number of variations in the computational model. A suitable probability distribution is fitted to each EDP based on simulation data, with distribution parameters derived accordingly. Statistical methods are then used to define the relationship between EDPs and IMs (Fig. 4). It is highlighted that for a building engineer, the demanding part is the construction of different variations of a model. This effort can be reduced by conducting sensitivity analysis or referring to existing studies in literature e.g. Ref. [45] to select the uncertain parameters mostly affecting the energy simulation results. The combined uncertainties in the weather hazard and the variability in the IM to EDP response are quantified by integration of the hazard curve $d\lambda(IM)$ over the conditional probabilities of G(EDP|IM) for the relevant range of IMs. This leads to the following mathematical expression of the Mean Annual Probability of exceeding a specified EDP, $\lambda_{EDP}(y)$ (Eq. (4)):

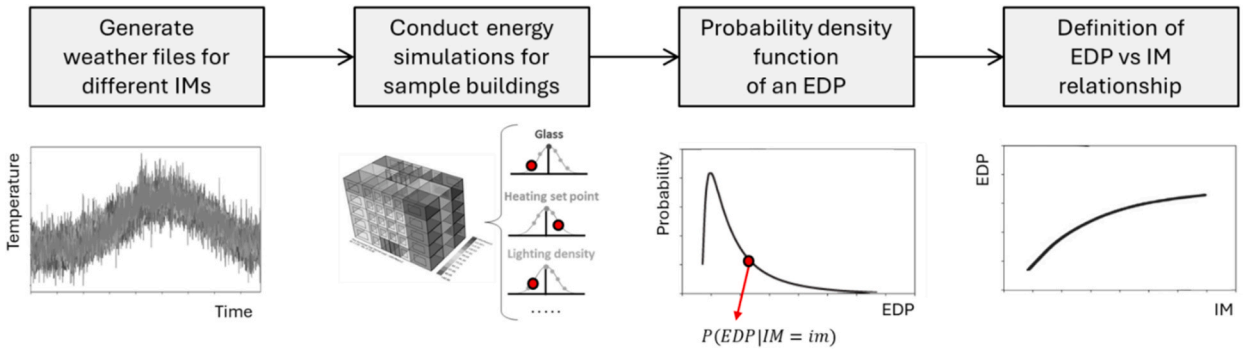


**Fig. 4.** Probabilistic building energy modelling.

$$\lambda_{EDP}(y) = \int P[EDP \geq y \mid IM = im] \left| d\lambda_{IM}(im) \right. \tag{4}$$

### 2.1.3. Fragility analysis

The probabilities of EDPs in the building analysis are used to determine the probability of exceedance of expected DV values. To do so, first fragility models should be derived, describing the probability of reaching or exceeding a specific response threshold level ($R_s$) for different values of EDP. Fragility functions typically take the form of lognormal cumulative distribution functions [46], having a median value, θ, and logarithmic standard deviation, or dispersion, β (Eq. (5)):

$$P(R \geq R_s|EDP) = \Phi\left(\frac{\ln\left(\frac{EDP}{\theta_i}\right)}{\beta_i}\right) \tag{5}$$

where $P(R \geq R_s|EDP)$ is the conditional probability that the system will exceed a certain value as a function of an engineering demand parameter; $\Phi$ denotes the standard normal (Gaussian) cumulative distribution function; $\theta_i$ denotes the median value of the probability distribution; and $\beta_i$ denotes the logarithmic standard deviation.

Uncertainty in the assessment stems from the threshold levels applied. In the context of thermal comfort, there is no universally accepted definition of overheating or acceptable indoor temperature limits. Further research is needed to establish health-based thresholds, particularly those that account for physiological risk. These thresholds may vary across different climates and demographic groups. For example, older adults often prefer warmer environments but may not perceive temperatures that are already physiologically harmful [47]. During heatwave periods, age, gender, income and also housing insulation are significantly associated with the heat perception [48]. Factors as occupants' social and health profiles, personal preferences, and acclimatization are challenging to obtain and model, introducing additional uncertainty into the assessment. Moreover, comfort thresholds can vary depending on environmental conditions, such as the combination of heat and humidity, which are difficult to predict, particularly under extreme or fluctuating scenarios.

### 2.1.4. Loss analysis

The quantification of the expected losses represents the last stage of the framework. The fragility information from the previous step is used to compute the final DVs, which can directly inform the design process and support stakeholder decision-making. The DVs can be represented in terms of *social loss*, associated with thermal discomfort and risk of casualties; *economic loss* due to energy consumptions and downtime during which the facility is not functioning for energy supply failures or decreased productivity due to not comfortable working conditions; *environmental loss* associated with the operation energy and air quality degradation. The probability of loss exceedance is assessed for individual thermal zones or the entire building, and the corresponding vulnerability curves (representing the variability of loss as a function of the IM) are quantified (see Section 3.2.4). The loss quantification is affected by different uncertainties, related to economic values such as fluctuation in the market prices and, especially, to the variation of human response to temperature levels, which is dependent on behavioral responses, human tolerance and physiological impacts, geographical and cultural differences. Efforts are currently underway to develop models for heat-related illnesses and deaths based on observed data from recent heatwaves e.g.Refs [49,50]. These uncertainties are propagated through the vulnerability model to generate the final loss curve, enabling quantification of the total expected probable losses.

DVs can be expressed in terms of annual frequencies of exceedance, λ(DV), which is a probabilistic description of the DV, such as the mean annual frequency of the DV exceeding a specified value. For example, λ(DV) might be the mean annual frequency of the energy cost exceeding 50% of a threshold value. Following the total probability theorem, where uncertainties in each aspect of the solution are described in terms of independent conditional probabilities, the λ(DV) can be derived using probabilistic integrals as follows (Eq. (6)):

$$\lambda(DV) = \iiint G\langle DV|RM\rangle \mid dG\langle RM|EDP\rangle \mid dG\langle EDP|IM\rangle \, d\lambda(IM) \tag{6}$$

Where G(EDP|IM), G(RM|EDP) and G(DV|DM), or their derivatives, are conditional probabilities relating one quantity to another, while dλ(IM), is the derivative of the hazard curve, relating the weather intensity measure to its mean annual frequency of exceedance. The equation implies for example, that given the demand described by EDP, the RMs are conditionally independent of the IM, i.e., the effects of weather are reflected in the calculated EDPs. If the continuous variables IM, EDP and RM are discretized into small intervals, the continuous integral can be approximated as (Eq. (7)):

$$P(DV) = \sum_i \sum_j \sum_k P(DV|RM_k)\, p\left(RM_k\middle|EDP^j\right)\; p\left(EDP^j\middle|IM_i\right)\; p(IM_i) \tag{7}$$

Where $p(IM_i)$ is the probability of occurrence of the ith value of IM (hazard analysis outcome), $p\left(EDP^j\middle|IM_i\right)$ is the probability of the jth value of EDP for the ith value of IM, $p\left(RM_k\middle|EDP^j\right)$ is the probability of the kth RM level when subjected to the jth value of the EDP used for the fragility function, $P(DV|RM_k)$ is the probability of exceedance of the DV value when the kth RM occurs.

This approach enables to derive expected annual losses for life-cycle economic planning, e.g., to evaluate the cost-benefits of designing a facility with higher performance targets versus opting for a lower performance target and purchasing insurance to cover

the added risk. However, another possibility is to use scenario-based expressions of DVs. In such cases, the probabilistic description of the loss DV might be described as having a confidence percentage that the losses would not exceed a certain value, assuming a certain predicted weather (a specific IM value). The framework therefore tracks the DV outcomes in a rigorous probabilistic way (Eqs. (6) and (7)), but also allows for translating this information into alternative forms (such as scenario-based analysis) that are more accessible to decision making of different stakeholders [51].

### 2.2. Framework application

The framework introduced in the previous section, adapted from the well-established PBEE methodology, represents a robust tool for building assessment and design, applicable to as-built, new construction and retrofit solutions. By quantifying expected probable losses, the framework integrates these metrics as key design and decision criteria. For instance, design objective matrices can be developed to define and target loss-based objectives for different building types, enabling discrete risk quantification as outlined in Section 2.2.1. Furthermore, loss estimates can be integrated into multi-criteria decision-making to define optimal building technologies at the early design stage, and the risk values derived from the probabilistic approach can be leveraged to guide decisions, as discussed in Section 2.2.2.

#### 2.2.1. Loss-based matrices

In engineering disciplines, performance-based design establishes how buildings would ideally perform under potential hazard events to achieve a target performance. The process considers uncertainties in hazard frequency and magnitude, as well as in the actual building response and potential impacts on building functionality. Performance-based design begins with the selection of design criteria, defined through performance objectives that represent acceptable building performance and the corresponding risk of losses due to building response; these objectives can be translated into design matrices (Fig. 5a). A key aspect in performance-based design is to validate the appropriateness of the selected performance (loss) levels, the parameters used to define their minimum performance and the hazard definitions [52]. Loss-based matrices that integrate hazard and consequences serve as valuable tools for guiding building design and retrofit against weather-related hazards. To ensure buildings meet specific performance standards, design criteria could be defined based on comfort, energy and environmental aspects [53]. Comfort focuses on creating healthy and comfortable indoor environments for occupants by ensuring adequate daylight, access to fresh air, maintenance of comfortable indoor temperatures and the absence of disturbing noise. Energy performance emphasizes the need for efficient energy use through optimized heating, cooling and lighting systems, as well as the adoption of renewable energy sources to reduce reliance on fossil fuels. Additionally, environmental impact plays a crucial role, requiring efforts to minimize negative consequences throughout the building lifecycle, including reduced resource consumption, waste generation and greenhouse gas emissions. Loss-based matrices can therefore be developed for all these dimensions, establishing specific quantitative thresholds informed by policy measures, technical guidelines or experimental data. For example, energy efficiency and operational energy thresholds can be defined based on energy performance standards for both new constructions and retrofit projects. These thresholds should account for local climate conditions, the availability of renewable energy sources and the involvement of local stakeholders [54]. Thermal comfort criteria can be drawn from literature studies or existing guidelines, such as ASHRAE Standard 55 [55] which provide benchmarks for acceptable thermal conditions based on factors like thermal sensation and stress levels. However, variability introduced by individual preferences, health conditions and acclimatization adds uncertainty to the design process.

By developing multi-dimension matrices (as shown in Section 3), designers can ensure that buildings are healthy, energy-efficient and environmentally sustainable based on expected hazard intensity levels. The resulting loss values ($DV$) can be also integrated into a weighted sum (Eq. (8)) to define a holistic risk value for the building, where the weights ($w$) can be defined based on the specific project and stakeholder preferences [56].

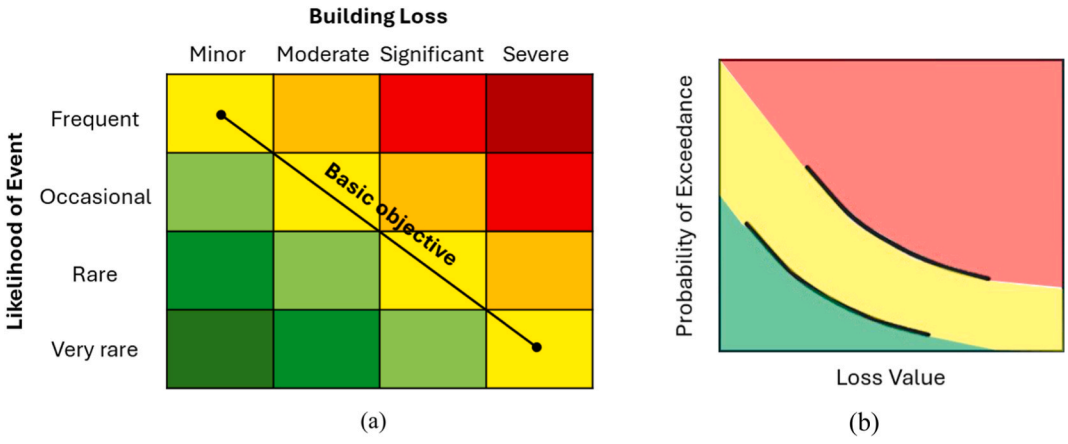


**Fig. 5.** (a) Loss-based matrix. (b) Loss curve.

$$R = \sum_i DV_i \, w_i \tag{8}$$

This risk value can then be used as a basis for comparing alternative building configurations, facilitating more informed and effective decision-making. It is noted that this paper does not aim to provide generalized design or risk matrices for buildings, as doing so would require specific investigations tailored to the climate and country under consideration. When analyzing a particular building configuration, once specific performance criteria are established and threshold levels defined, the framework herein outlined can be employed to quantify the expected probable losses and determine whether the performance meets acceptable standards or risk levels.

#### 2.2.2. Quantitative risk assessment

The proposed probabilistic approach allows the characterization of building heat vulnerability (expected loss vs. heat hazard) and the quantification of associated risk. Risk is calculated by multiplying the probability of hazard, vulnerability and exposure, with the latter related to e.g. the number of impacted people and the urban context properties. This calculation yields a dimensionless value for the risk level, which is often used for scenario comparisons and sensitivity analyses. However, this value lacks a specific physical meaning, making it challenging to effectively communicate to stakeholders. To address this, catastrophe modelling typically express risk through exceedance probability curves (derived from the proposed framework, and more commonly called loss curves) and associated risk metrics, which are more tangible and can inform risk management decisions. An exceedance probability curve provides detailed insights into the potential impacts caused by extreme events for a specific building. A key risk metric is the EAL value (Eq. (9), Fig. 5b), representing the area under the loss curve.

$$\lambda_{DV}(y) = \int P[DV \geq y \,|IM = im] \, d\lambda_{IM}(im) \tag{9}$$

This metric forms the basis for assessing financial risk for disasters (e.g. seismic, flood, windstorms) and is crucial for determining appropriate mitigation strategies, such as insurance premiums or adaptation measures. The PBEE therefore enables to quantify EAL through a careful evaluation of building performance, a critical step through which hazards are translated into “loss” (such as fatalities, typically used in disaster impact assessment). Another important metric is the value at risk, which corresponds to a quantile of the loss distribution at a chosen confidence level (e.g. 90%), and the probability of exceeding a particular loss level to help assess the likelihood of severe impacts on the building [57].

## 3. Practical implementation

### 3.1. Case study definition

#### 3.1.1. Building data

A case study building is used to demonstrate the application of the probabilistic framework introduced in the previous section. The case study involves a multi-story residential building representative of a typical pre-1970 reinforced concrete building in Italy. Buildings from this construction period account for a substantial share of the Italian residential stock (approximately 51% [58]), mostly built prior to the introduction of thermal insulation regulations. As a result, this building typology is characterized by poor thermal performance and high vulnerability to heat stress, making it a relevant and representative case for demonstrating the proposed framework.

The building consists of reinforced concrete frames with infilled brick masonry walls and has a total floor area of 794 $m^2$. Detailed construction characteristics and thermal properties (transmittance, U-values), summarized in Table 1, are derived from the TABULA

**Table 1**
Building properties from TABULA project [59].

| Building class | Construction period | Floor area [$m^2$] | Component | Type | U-value [W/($m^2$K)] | Services |
|---|---|---|---|---|---|---|
|  Multi-family house | 1961-1975 | 794 | Wall  | Hollow wall brick masonry | 1.15 | no ventilation system; gas central heating |
| | | | Window  | Single glass, wood frame | 4.90 | |
| | | | Floor  | Reinforced brick-concrete slab | 0.94 | |
| | | | Roof  | Reinforced brick-concrete slab | 1.10 | |

project [59], ensuring consistency with standardized European residential building archetypes. The building comprises six mid-rise apartments and shared corridors on each floor, occupied by a diverse age range of residents from 25 to over 80 years old. It is located in a typical urban neighborhood of Messina, surrounded by 3-5 story residential and mixed-use buildings with moderate street widths. Small green areas, such as courtyards and street-side vegetation, are present in the vicinity, while prevailing coastal breezes from the Strait of Messina support natural ventilation. Due to this configuration, the surrounding urban context exerts a limited impact on the building's thermal performance and exposure to heat. The energy demand for space heating and domestic hot water is approximately 115 kWh/m$^2$year, while the total primary energy demand is 220 kWh/m$^2$year, based on climatic conditions in a temperate zone (Zone E, as defined by DPR 26-8-1993 n. 412 [60]). This information is used for validating the building energy results, as discussed in Section 3.2.2.

### *3.1.2. Weather data*

The building is assumed to be located in Messina, which has a warm temperate Mediterranean climate characterized by hot, dry summers and mild, wet winters. According to the Köppen-Geiger Climate Classification, this corresponds to the "Csa" category. The Mediterranean region is particularly vulnerable to climate change and is already experiencing a noticeable increase in the demand for cooling in residential buildings [61]. A preliminary analysis of historical weather data was conducted using records from NOAA's online database [62], based on observations from the Messina weather station (IWEC 164200), which is representative of the local climatic conditions for this building-scale heat risk study. These datasets include multiple weather parameters relevant for energy simulations, such as outdoor temperature, relative humidity, solar radiation. Data were processed to generate EPW files (EnergyPlus [44] Weather Files) for dynamic energy simulations, using the Dragonfly plugin in Grasshopper environment (running within the Rhinoceros application [63]) to adjust raw climate data by reconstructing horizontal infrared radiation and sky illuminance for accurate thermal simulation inputs. The historical data were compared with a Typical Meteorological Year (TMY) file, which consist of one year of hourly data representing median weather conditions over a multiyear period [64]. Analysis revealed an average annual dry bulb temperature of 19 °C for Messina. An increasing trend in Cooling Degree Days (CDD) was observed, which represent the number of degrees by which a day's mean temperature exceeds a base temperature of 18 °C, suggesting rising cooling demand. In contrast, Heating Degree Days (HDD), defined as the number of degrees below the same base temperature, are decreasing (Fig. 6a). The dataset also showed interannual variability by computing coefficient of variation (CoV), i.e. the ratio of the standard deviation to the mean, for key parameters: (1) temperature, relative humidity and global solar radiation are all characterized by CoV values less than or equal to 0.05, indicating low variability; (2) in contrast, direct normal radiation and wind speed show higher variability, with CoV values of 0.13 and 0.18, respectively.

In addition to historical weather records, future climate projections were also incorporated into the analysis. Specifically, future weather scenarios were generated using the Future Weather Generator tool [65], which morphs the historical TMY EPW file to reflect projected changes due to climate change and the UHI effect. This tool employs outputs from 20 Global Circulation Models (GCMs) and considers three Shared Socioeconomic Pathways (SSPs) - SSP2-4.5, SSP3-7.0, SSP5-8.5 - across two future timeframes: mid-century (2050: 2036–2065) and late-century (2080: 2066–2095) [66]. The morphing process adjusts present-day hourly EPW files used in dynamic simulations to match the projected climate conditions, including UHI effects. While this method effectively incorporates long-term climatic trends and inter-model uncertainty, it may underestimate the intensity and frequency of extreme heatwave events, meaning actual future risks could be more severe. To address the uncertainty associated with climate projections, all 20 GCMs across the three SSPs and two timeframes were considered (e.g., Fig. 6b for dry bulb temperature projections), resulting in a total of 120 future weather files (20 GCMs for each SSP and future timeframes). When analyzing the variability in annual mean values across these future files, results showed similar CoV to those observed in historical data, with wind speed only exhibiting lower CoV values, approximately 0.05–0.06, indicating relatively consistent trends across models.

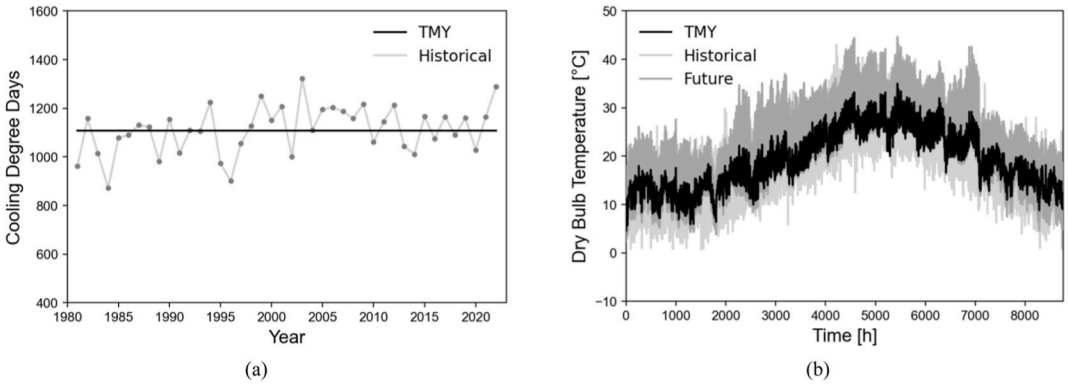


**Fig. 6.** (a) Trend in historical data for the city of Messina, Italy.(b) Annual dry bulb temperature data, including future projections across all SSP scenarios and timeframes (2050, 2080).

### 3.2. Probabilistic loss estimation

#### 3.2.1. Hazard analysis

To build site-specific hazard curves, historical data were processed by computing the empirical cumulative distribution function and deriving the corresponding annual probability of exceedance, as described in Section 2.1.1. Using extreme dry-bulb temperature as the IM, a Gumbel extreme value distribution (consistent with ASHRAE guidelines [67]) can be fitted to the annual maximum data. The mean and standard deviation of the dataset are used to define a continuous probability function describing the exceedance of temperature extremes. Fig. 7a presents the resulting hazard curve validated against ASHRAE [67] temperature values for Extreme Annual Design Conditions (EADC), showing a close agreement. A hazard curve based on this IM can be used by designers and engineers to identify the maximum temperatures expected at a site, informing the design of critical mechanical equipment in buildings. It is noteworthy that the hazard curve derived from historical data yields a temperature of 40 °C associated with an annual probability of exceedance of 0.02 (i.e., a value exceeded on average once every 50 years). This value is consistent with the characteristic temperature specified in the Italian national code [68], which is also equal to 40 °C for buildings assumed to be located at sea level (0 m a.s.l.) and is based on long-term climatic records. Although such temperature values are primarily used as design parameters for structural thermal actions, they represent extreme design conditions corresponding to rare exceedances, which are consistent with the hazard curve definition adopted in this paper.

Hazard curves for different climate scenarios are also derived (Fig. 7b), with the SSP3-7.0 scenario for 2050 showing lower values than SSP2-4.5 due to inter-model variability across the ensemble of GCMs used. These hazard curves are generated by shifting the mean of the Gumbel distribution according to projected future maximum temperatures, while keeping the historical standard deviation unchanged. This approach isolates the effect of mean temperature shifts and is adopted due to the unavailability of multi-year EPW datasets for the analyzed location. As discusses above, the projected datasets are derived from the TMY file, which may underestimate extreme heatwaves. When multi-year datasets that include heatwave events are available for future timeframes, such as those derived for certain locations by the Annex 80 working group [69], the same empirical approach used for the historical data can be applied to capture the evolving hazard profile under climate change.

The same approach for hazard-curve derivation can be extended to other IMs, with the choice of IM guided by the specific loss outcome and problem under investigation. It is not a fixed predefined parameter; rather, its selection is an integral part of the risk assessment procedure. For example, the HI, which combines air temperature and relative humidity to reflect perceived temperature [70], can be adopted as an IM and used as a rapid screening tool for assessing heat-related risks associated with indoor thermal comfort and occupant health. The National Weather Service (NWS) [71] provides a chart linking HI values to the likelihood of heat-related illnesses under prolonged exposure or intense activity. Applying this methodology to the current location, enables an initial assessment of climate change impacts, as illustrated in Fig. 8. The results indicate that, according to the design return periods defined by ASHRAE [65], the current climate reaches the "extreme danger" threshold for a return period of 50 years. Under higher and more extreme emission scenarios, this threshold is projected to be reached as frequently as every 10 years.

In this study, CDDs were selected as the IM because they capture both the intensity and duration of outdoor temperatures relative to a base threshold, providing a cumulative indicator of prolonged thermal stress experienced by buildings and HVAC systems. CDDs are therefore directly linked to building energy demand and thermal-related losses, making them particularly suitable for the estimation of annualized losses (i.e., EAL), for aggregation over time and for the definition of fragility functions (e.g., Ref. [28]).

#### 3.2.2. Building analysis

To probabilistically quantify the building response to heat hazards (Section 2.1.2), a model was developed in EnergyPlus [44] to conduct dynamic energy simulations, incorporating the physical and operational characteristics summarized in Table 1. The building envelope, comprising walls, roofs, floors and windows, was explicitly modelled by assigning thermal properties such as conductivity, specific heat, density and emissivity. The building was divided into thermal zones based on residential occupancy patterns and thermal behavior. This zoning strategy allows the simulation to capture dynamic interactions between building components and the HVAC

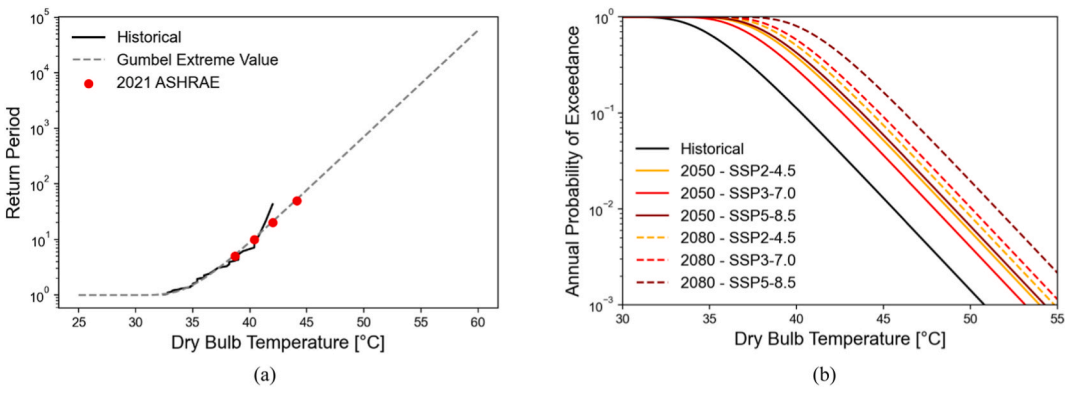


**Fig. 7.** (a) Cumulative distribution from historical data. (b) Hazard curves considering all SSPs scenarios.

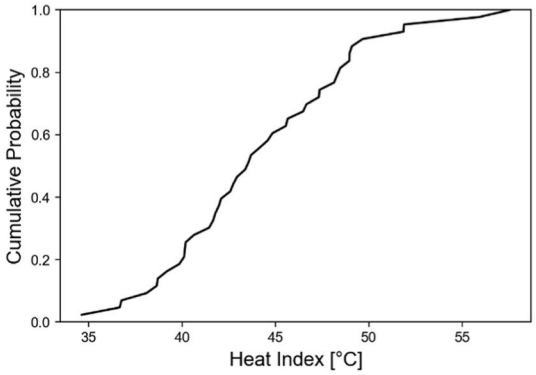


(a)

| Return period [years] | Historical [°C] | Future (SSP5-8.5) [°C] |
|---|---|---|
| 5 | 48.44 | 51.79 |
| 10 | 50.62 | 53.98 |
| 20 | 52.43 | 55.78 |
| 50 | 54.46 | 57.82 |

Danger (41-54 °C)

*Sunstroke, muscle cramps, and/or heat exhaustion likely. Heatstroke possible with prolonged exposure and/or physical activity*

Extreme danger (54 °C or higher)

*Heat stroke or sunstroke likely*

(b)

**Fig. 8.** (a) Empirical cumulative distribution for Heat Index from historical data. (b) Heat Index values for the current vs future weather (extreme scenario: SSP5-8.5), considering the classification provided by NWS [71].

system. The HVAC system was modelled using the Ideal Loads Air System in EnergyPlus, which assumes perfect efficiency and excludes system losses (air-conditioning system is assumed to have a COP of 2.9). The maximum cooling capacity was defined by the peak cooling load calculated for the design day at the specific location. Thermal comfort was maintained using fixed setpoint temperatures: 26 °C for cooling and 20 °C for heating. Internal heat gains were defined as 2 W/m$^2$ for equipment, 10 W/m$^2$ for lighting and an occupant density of 0.02 persons/m$^2$. In addition to air infiltration (0.0003 m$^3$/s per m$^2$ of floor area), natural ventilation through operable windows was included in the model. These airflow mechanisms were accounted for in energy simulations to estimate their impact on cooling demand and thermal comfort. To validate the simulation results, energy performance was compared against the primary energy consumption of 115 kWh/m$^2$·year (and associated energy costs and carbon emissions) reported for the archetype building in the TABULA database for climatic zone E [59]. Using TMY files for Italian cities in Zone E (e.g., Perugia), the comparison showed very good agreement, with the model yielding a primary energy consumption of 117-120 kWh/m$^2$·year, corresponding to a difference of approximately 1-2% under the same climate conditions.

Following model validation, simulations were further pre-processed to incorporate climate variability and automate batch runs using Python. This initial study does not account for uncertainties in building properties or occupant behavior; but instead isolates the impact of climate variability on building performance. Moreover, two complementary design configurations were considered for the building: (i) a model with mechanical cooling to quantify energy demand, and (ii) a model relying solely on natural ventilation (via operable windows) to assess indoor thermal conditions and passive survivability during heat events. This dual approach highlights the importance of considering both active cooling strategies and passive building resilience when evaluating heat risk and occupant exposure. Simulation outputs were used to derive Energy Use Intensity (EUI) and Standard Effective Temperature (SET), that are key indicators for energy efficiency and thermal comfort and are considered as RMs in this study (following the approach illustrated in

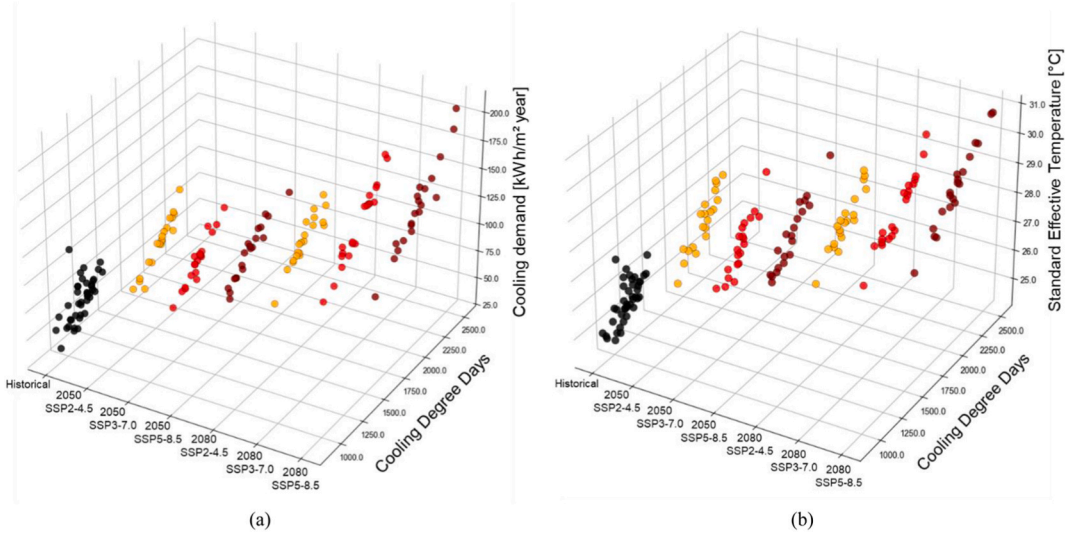


(a) (b)

**Fig. 9.** Increase in (a) cooling energy demand (under mechanical cooling) and (b) thermal comfort stress (under natural ventilation) in response to climate variability.

Fig. 2).

EUI measures a building's total energy consumption relative to its floor area, encompassing heating, cooling, lighting and equipment loads. SET, on the other hand, is calculated based on indoor air temperature and mean radiant temperature and is defined as the dry-bulb temperature in an environment with 50% relative humidity, where the human body would experience the same thermal stress as in the actual environment [55]. Results show that projected climate conditions lead to a marked increase in both indicators, particularly evident in the increased cooling energy demand driven by the rise in CDD over time for the analyzed location (Fig. 9).

### 3.2.3. Fragility analysis

To generate fragility curves for the building (Section 2.1.3), the Cloud Method [72] was employed following the approach for thermal fragility functions proposed by Kim et al. [73]. This method applies a linear regression on a logarithmic scale between Demand-to-Capacity Ratios (DCRs) and the selected IM, which in this study is CDD for building-level analysis (and/or the relevant EDP when analyzing individual thermal zones or floor levels; Fig. 1). For energy performance, DCRs are calculated as the ratio of the EUI results to a predefined threshold. The threshold corresponds to the Class D energy labelling limit (130 kWh/m$^2$, based on data from Calvi et al. [74]) for residential buildings, corresponding to the lower bound of acceptable energy efficiency for residential buildings in Italy. For thermal comfort, thresholds are defined based on human thermal sensation and physiological responses. A SET of 30 °C is considered a threshold for warm, uncomfortable and potentially unsafe conditions inducing sweating, according to Wenjie et al. [75]. The resulting DCRs vs. CDD curves (Fig. 10a and c) show that the EUI exhibits about 30% greater dispersion, indicating higher variability in this performance metric compared with the SET values.

The linear regression models are used to derive the median and logarithmic standard deviation, which are then applied in Eq. (5) to generate the building-level fragility curves (Fig. 10b and d), representing the probability of reaching or exceeding the defined thresholds. These curves reflect the dispersion observed across multiple simulation runs, and include an additional uncertainty to account for physics-based numerical modelling and underlying assumptions. Following existing PBEE frameworks (e.g. FEMA P-58 [57]), lognormal standard deviations in the range 0.1-0.3 are commonly used to represent such uncertainty. Accordingly, a value of 0.15 was adopted to derive the combined standard deviation (square root of the sum of the squares of the individual standard deviations, simulation variability and modelling) of the fragility curves.

### 3.2.4. Loss analysis

Heat-related consequences (loss functions) are estimated by propagating uncertainty from the fragility and consequence models through a Monte Carlo simulation framework (Fig. 11). The procedure consists of four main steps.

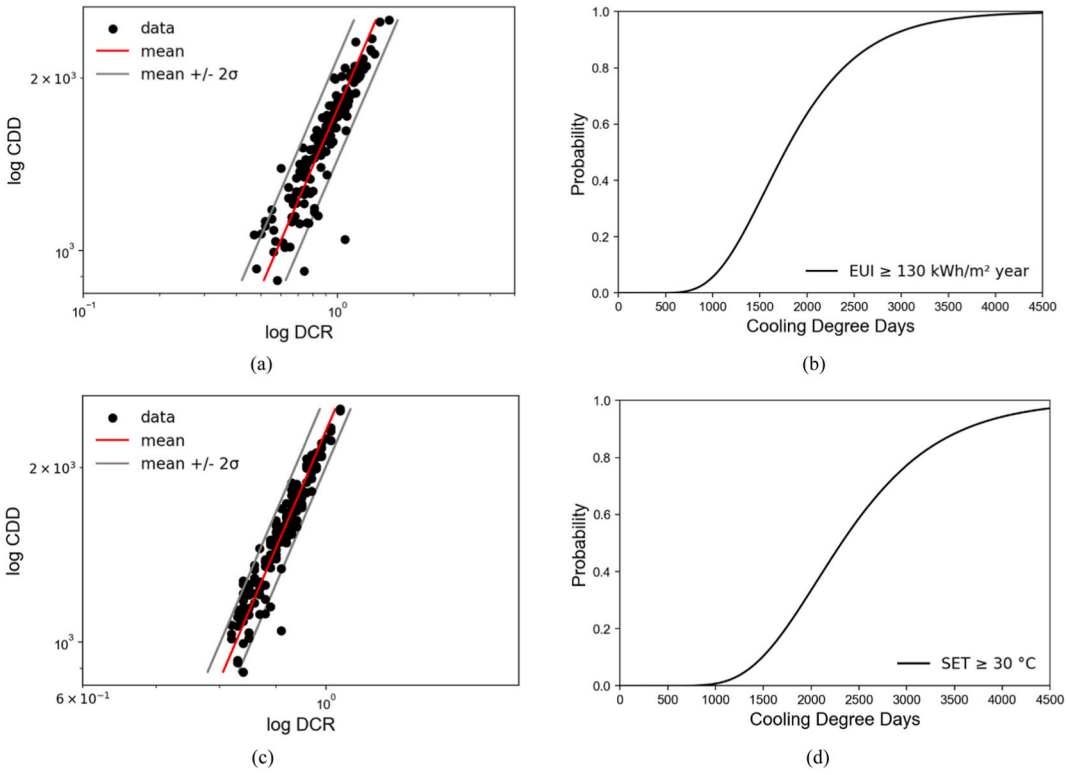


**Fig. 10.** IM-DCR relationships and corresponding fragility curves for (a, c) unacceptable energy efficiency degradation (under mechanical cooling) and (b, d) thermal comfort conditions (under natural ventilation).

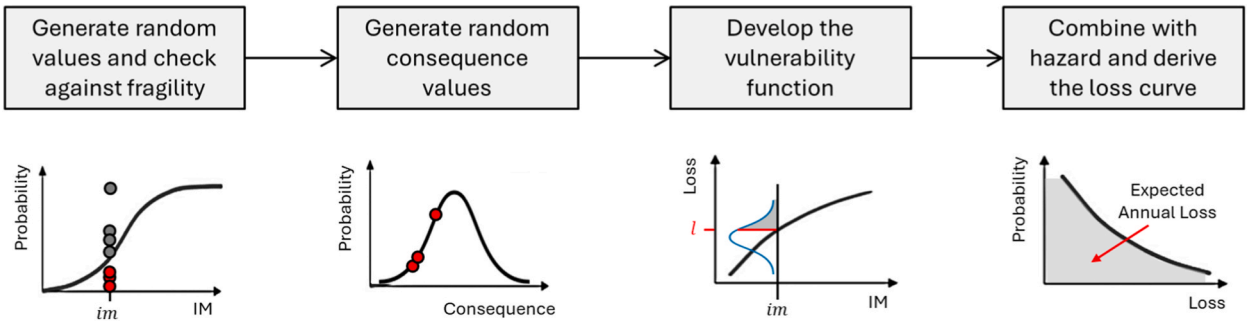


**Fig. 11.** Propagation of uncertainties to derive loss curve.

- *Step 1.* For each IM value, random numbers between 0 and 1 are generated using the Latin Hypercube Sampling method. These values are interpreted as exceedance probabilities and are mapped onto the fragility curve to determine whether the corresponding threshold is exceeded. In this application, a single fragility function representing a severe condition is considered (Fig. 10). If multiple thresholds are available, each random value is evaluated against all corresponding fragility curves.
- *Step 2.* When a sampled value lies on or below the fragility curve, a second random value is drawn from the assumed consequence distribution (as defined in Table 2) to represent a realization of heat-related loss.
- *Step 3.* The vulnerability relationship is constructed by linking the IM values from Step 1 to the corresponding loss realizations from Step 2. For each IM, the ensemble of simulated losses defines a probabilistic distribution (represented by the vertical slices of the vulnerability curve). The mean of these distributions defines the vulnerability curve, while the spread represents uncertainty.
- Step 4. The final loss curve is obtained by combining the vulnerability model with the hazard curve using a discretized form of Eq. (7) adapted for building-level assessment (Fig. 2). The hazard exceedance curve (annual probability of exceedance vs CDDs) is first converted into probability bins, $p(IM_i)$, representing the likelihood that the hazard falls within successive intensity intervals. For each IM (CDD), the conditional probability that losses exceed a given threshold (l value in the vulnerability curve of Fig. 11) is computed and weighted by the corresponding hazard probability. Applying the total probability law (Eq. (7), Section 2.1.4), this

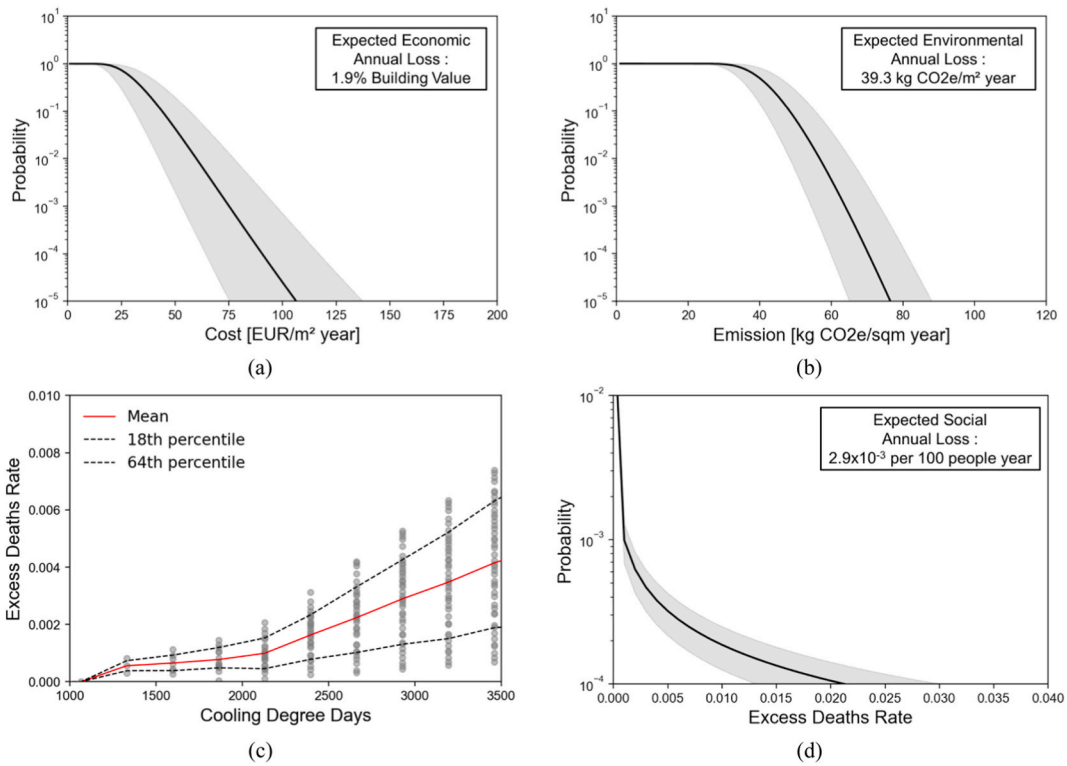


**Fig. 12.** Loss curves showing mean and uncertainty bounds (16th and 84th percentiles) for (a) energy cost and (b) operational carbon (under mechanical cooling); (c) vulnerability and (d) loss curve for heat-related deaths (under natural ventilation).

convolution yields the loss exceedance curve, which expresses the annual probability that heat-related consequences exceed any given level. The expected annual loss value (EAL) is then obtained as the area under this curve.

In this application, the EUI-based fragility curve is used to derive both economic and environmental loss curves. However, if a specific operational carbon threshold is of interest, a fragility curve corresponding to that limit can instead be employed for the environmental impact assessment. Social losses are assessed through the fragility curve derived from the SET indicator. In particular, SET is used to identify Monte Carlo realizations in which indoor thermal conditions reach potentially unsafe levels. Once such realizations are identified, excess mortality is estimated using the functions proposed by Masselot et al. [50], which provide the range of excess death rates based on historical temperature data and future projections. In this study, functions for all age groups (20-85+) are used, assuming no adaptation and therefore no risk attenuation.

Consequence uncertainties (Step 2) are modelled using the probability distributions summarized in Table 2. For energy costs, the distribution is defined following the work by Sun et al. [12], with the mean based on current prices provided by Eurostat for Italy. For the total natural gas emission factor, both methane combustion and supply-chain leakage are considered. The combustion component is only marginally variable and is therefore treated as deterministic (0.198 kg $CO_2$/kWh). Variability in upstream emissions is modelled using a lognormal distribution to capture uncertainty across supply-chain stages. The mean of this distribution is set to 0.10 kg $CO_2$/kWh, based on the upper range reported by Balcombe et al. [76] for typical facilities. The two contributions are then summed to obtain the total emission factor. This approach ensures that the lower bound of total emissions converges toward the combustion-only value, while the right-skewed distribution appropriately reflects the asymmetric risk of higher emissions under less optimal supply-chain conditions. Using these distributions, the final cost and emission curves enable quantification of the expected economic (expressed as a percentage of the building's total value - assumed here as 1600 EUR/$m^2$ [30]) and environmental annual losses, represented by the area under the loss curves (Figs. 12a and 10b). For the excess death rate, random values are generated at each iteration between the minimum and maximum rates reported by Masselot et al. [50] and summarized in Table 3. The table shows a negative value for the heat excess death rate in 2050 and a slightly higher estimated rate in 2050 compared to 2080. These outcomes reflect statistical and demographic modelling effects, since the estimates are based on age-specific vulnerability functions applied to projected population distributions, which can produce small aggregate fluctuations over time. These sampled values are then used to construct the vulnerability curve (Fig. 12c; excess death rates vs. CDD values), from which the corresponding loss curve and the expected annual loss of life are derived (Fig. 12d).

### 3.3. Performance evaluation

#### 3.3.1. Loss-based matrices

The vulnerability analysis results enable the quantification of weather-related impacts to inform building decision-making. Specifically, the approach described in the previous section allows for assessing how a building's performance deteriorates in terms of energy efficiency, by computing expected energy costs and operational carbon emissions. The analysis also captures how the building may become unsafe over time, potentially leading to health-related issues. This can be assessed using the Relative Risk (*RR*) associated with heat-related mortality. *RR* is calculated based on the excess death rate ($D_{Excess}$) compared to the baseline death rate ($D_{Baseline}$), which represents mortality during a reference period without heat exposure:

$$RR = 1 - \frac{D_{Excess}}{D_{Baseline}} \tag{10}$$

Following a risk matrix approach, this information can be used to compare the impact of climate change for the building under consideration. Multi-domain matrices can be structured around the return periods for extreme temperatures defined by ASHRAE [67], which correspond to the annual extreme design conditions. For each impact domain, specific performance thresholds are established. For energy cost, classification follows the energy labelling system proposed by Calvi et al. [74], which uses the so-called Green Indicator. The classification aligns with thresholds for Classes A, B and C, reflecting increasing levels of energy-related financial burden. For the operational Global Warming Potential (GWP), threshold values are derived from the primary energy levels by applying appropriate emission factors for grid electricity (0.35 kg $CO_2$-eq/kWh) and natural gas (0.202 kg $CO_2$-eq/kWh) specific to Italy. Regarding the *RR* thresholds, no universally accepted classification exists; however, the following values are used to indicate escalating levels of health risk: 1.2 for operational threshold - heat likely contributing to excess mortality; 1.5 for high increase - often linked to heatstroke or prolonged heat exposure; 2.0 for severe risk - mortality rate doubles compared to baseline. After constructing these matrices, the loss values obtained for all return periods using the PBBE-based framework (as shown in Table 4) can be used to position

**Table 2**
Cost and emission probabilistic distributions.

| Consequence | Distribution | Mean | Coefficient of Variation | Reference |
|---|---|---|---|---|
| Energy cost | Log-normal | 0.33 EUR/kWh | 0.18 | Eurostat, Sun et al. [12] |
| Gas cost | Log-normal | 0.10 EUR/kWh | 0.09 | Eurostat, Sun et al. [12] |
| Emission factor (supply chain) | Log-normal | 0.10 kg $CO_2$/kWh | 0.44 | Balcombe et al. [76] |

**Table 3**
Heat excess deaths rates for selected years derived from Masselot et al. [50] (for Italy, SSP2-4.5, all age groups, no adaptation).

| Year | Low rate | High rate | Estimated rate |
|---|---|---|---|
| 2020 | 2.71E-05 | 0.000436 | 0.000200982 |
| 2050 | −2.77E-06 | 0.001166 | 0.00054509 |
| 2080 | 8.42E-05 | 0.001217 | 0.000523185 |

**Table 4**
Loss values (mean, 16th and 84th percentiles) for the current climate (1980-2025).

| Return Period | Energy cost [as a % of Building Value] | | | Operational GWP [kg $CO_2e/m^2$ year] | | | Relative Risk | | |
|---|---|---|---|---|---|---|---|---|---|
| | mean | 16th pct | 84th pct | mean | 16th pct | 84th pct | mean | 16th pct | 84th pct |
| 5 years | 1.43 | 1.02 | 1.82 | 30.60 | 26.01 | 35.04 | 0.49 | 0.21 | 0.76 |
| 10 years | 1.45 | 1.04 | 1.84 | 30.92 | 26.29 | 35.41 | 0.60 | 0.26 | 0.93 |
| 20 years | 1.46 | 1.05 | 1.86 | 31.23 | 26.55 | 35.76 | 0.70 | 0.30 | 1.09 |
| 50 years | 1.48 | 1.06 | 1.89 | 31.63 | 26.89 | 36.22 | 0.83 | 0.36 | 1.30 |

the building's performance within the risk matrices, enabling verification of whether thresholds of interest are exceeded.

By estimating losses (e.g. mean values) across all climate scenarios, a progressive increase in impacts can be observed (Fig. 13), leading to relative shifts in performance levels when represented within the proposed risk matrices (intended to support comparative assessment across scenarios for the case study building). For instance, the RR associated with heat-related mortality shifts toward higher impact for events with a 5-year return period, indicating that this consequence metric is more sensitive to increasing heat hazard compared to others within the adopted classification scheme. However, it should be noted that the *RR* computed values are conservative, as they are based on a baseline mortality rate corresponding to the maximum demographic death rate projected by Masselot et al. [50]. This baseline reflects national-level data for all age groups across Italy, rather than region-specific figures or the demographics of the actual building occupants.

For the selected case study, analysis across all scenarios, summarized in Tables 5–7, reveals the following trends.

- Energy degradation costs increase steadily across all return periods and scenarios relative to historical baselines. By 2050, values clearly exceed the 1.5% building-value threshold under every SSP pathway, implying a downgrade from Class B. Extending the return period from 5 to 50 years produces an additional 2-3% relative increase, related to 200-300 additional CDDs. Compared with historical baselines, costs reach up to 13% higher by 2080 SSP5-8.5.
- Carbon intensity increases across all return periods and scenarios. By 2050, operational GWP is roughly 7% higher than historical levels, and by 2080 it reaches up to 13% under SSP5-8.5. The influence of the return period is consistent but relatively modest, highlighting that long-term climate change, rather than the frequency of extreme events, is the primary driver of higher operational carbon intensity.
- Death rates increase substantially across all return periods and scenarios. By 2080, under SSP5-8.5, the RR rises from 0.49 to 1.67, representing an increase of over 200% across the selected return periods. Even under the moderate SSP2-4.5 pathway, RR nearly doubles or triples, indicating that heat-related health impacts remain significant. Extending the return period from 5 to 50 years adds an additional ~20% increase within each scenario.

Finally, it is observed that the 2050 SSP3-7.0 scenario shows slightly lower values than SSP2-4.5 in some indicators. As discussed in the previous section, this is due to inter-model variability across the ensemble of GCMs used. Such differences, especially in near-term

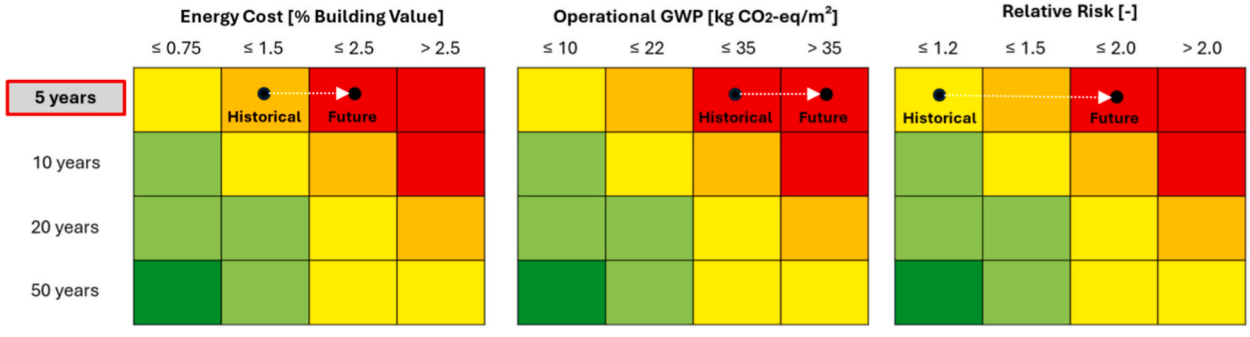


**Fig. 13.** Multi-dimensional risk matrices and performance change of the analyzed building for a 5-year return period under current vs future climate (2080 SSP5-8.5).

**Table 5**
Energy cost (mean value, as a % of Building Value) (under mechanical cooling).

| Return Period | Historical (1980-2025) | 2050 (2036–2065) SSP2-4.5 | 2050 (2036–2065) SSP3-7.0 | 2050 (2036–2065) SSP5-8.5 | 2080 (2066–2095) SSP2-4.5 | 2080 (2066–2095) SSP3-7.0 | 2080 (2066–2095) SSP5-8.5 |
|---|---|---|---|---|---|---|---|
| 5 years | 1.43 | 1.53 | 1.52 | 1.54 | 1.57 | 1.59 | 1.63 |
| 10 years | 1.45 | 1.54 | 1.54 | 1.56 | 1.59 | 1.61 | 1.64 |
| 20 years | 1.46 | 1.56 | 1.55 | 1.57 | 1.60 | 1.62 | 1.66 |
| 50 years | 1.48 | 1.57 | 1.57 | 1.59 | 1.62 | 1.64 | 1.68 |

**Table 6**
Operational Global Warming Potential (mean value, in kg CO2e/$m^2$ year) (under mechanical cooling).

| Return Period | Historical (1980-2025) | 2050 (2036–2065) SSP2-4.5 | 2050 (2036–2065) SSP3-7.0 | 2050 (2036–2065) SSP5-8.5 | 2080 (2066–2095) SSP2-4.5 | 2080 (2066–2095) SSP3-7.0 | 2080 (2066–2095) SSP5-8.5 |
|---|---|---|---|---|---|---|---|
| 5 years | 30.60 | 32.65 | 32.51 | 32.96 | 33.59 | 34.12 | 34.88 |
| 10 years | 30.92 | 32.97 | 32.83 | 33.28 | 33.91 | 34.45 | 35.20 |
| 20 years | 31.23 | 33.27 | 33.14 | 33.59 | 34.22 | 34.75 | 35.51 |
| 50 years | 31.63 | 33.67 | 33.54 | 33.99 | 34.62 | 35.15 | 35.91 |

**Table 7**
Relative risk values (mean value) (under natural ventilation).

| Return Period | Historical (1980-2025) | 2050 (2036–2065) SSP2-4.5 | 2050 (2036–2065) SSP3-7.0 | 2050 (2036–2065) SSP5-8.5 | 2080 (2066–2095) SSP2-4.5 | 2080 (2066–2095) SSP3-7.0 | 2080 (2066–2095) SSP5-8.5 |
|---|---|---|---|---|---|---|---|
| 5 years | 0.49 | 1.02 | 0.98 | 1.11 | 1.30 | 1.45 | 1.67 |
| 10 years | 0.60 | 1.12 | 1.08 | 1.21 | 1.39 | 1.55 | 1.77 |
| 20 years | 0.70 | 1.21 | 1.17 | 1.30 | 1.48 | 1.64 | 1.85 |
| 50 years | 0.83 | 1.32 | 1.28 | 1.41 | 1.60 | 1.75 | 1.97 |

projections, underscore the need for using multiple models to account for uncertainty.

### *3.3.2. Expected annual loss*

For energy costs and operational energy, besides considering exceedance of a specific energy efficiency degradation level, the total annual energy consumption can be computed to reflect the building's continuous performance. This approach moves beyond the traditional reliance on fragility functions and directly uses the established relationship between the EDP (energy demand) and IM (CDD) (Fig. 14a). Using a Monte Carlo approach, for each realization of the IM an EDP is randomly sampled from a lognormal distribution, representing the uncertainty in energy demand for a given hazard intensity. The sampled EDP is then translated into energy use (EUI) and combined with a randomly sampled unit energy cost, also modelled as a lognormal distribution (Section 3.2.4), to estimate the total economic loss (Fig. 14b).

The final loss curve can be derived for all hazard scenarios (e.g., Fig. 15a), enabling the estimation of total annual economic losses

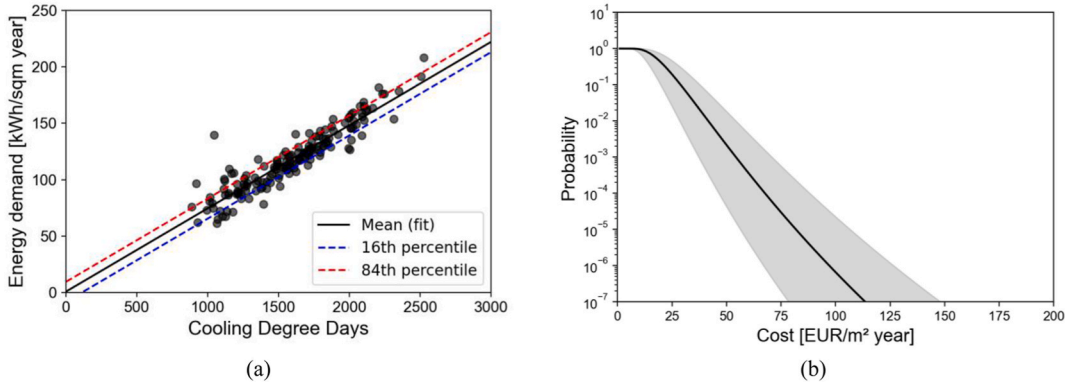


**Fig. 14.** (a) Energy demand - Cooling Degree Days relationship, (b) Loss curve for total energy cost, including uncertainty bounds (16th and 84th percentiles) (under mechanical cooling).

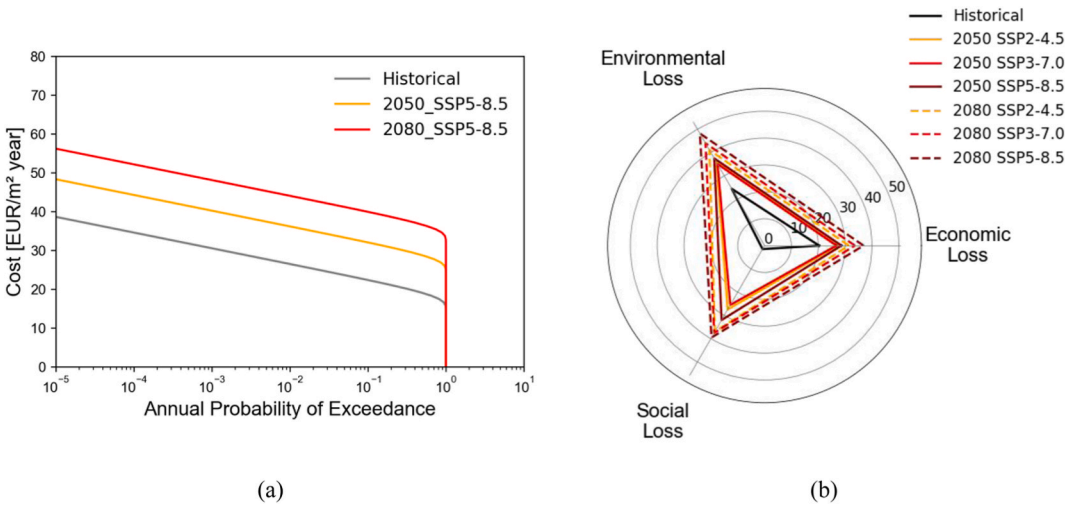


**Fig. 15.** (a) Economic loss curves (under mechanical cooling) for 2050 and 2080 (SSP5-8.5). (b) Radar chart comparing the consequences of climate scenarios (where the social loss values have been scaled by a factor of 500 for visualization purposes).

and operational carbon emissions as the area under each curve. Combined with the annual loss of life from heat hazards, these outcomes enable a comprehensive assessment of the building vulnerability and projected climate change impacts. For the case study, the results reveal that (Table 8): (i) annual economic losses are projected to increase by approximately 40% by 2050, and by up to 80% by 2080, particularly under high-emission scenarios (SSP5-8.5), emphasizing the escalating financial burden of climate inaction; (ii) the operational carbon footprint follows a similar trajectory, with values projected to double by 2080, reinforcing the conclusion that climate-induced performance degradation poses a significant threat to achieving decarbonization targets; (iii) a sharp rise in mortality risk, indicating that health-related impacts (those from overheating or unsafe indoor conditions) could become a major concern. These annualized losses, calculated as the area under the mean loss curves from the Monte Carlo approach, account for uncertainties in the vulnerability assessment and can be visualized in a single radar chart (Fig. 15b), allowing for a direct comparison of expected risks across different impact metrics. The shape and extent along each axis provide an intuitive representation of the relative magnitude of each loss component, offering a visual overview of the building's vulnerability to heat hazards.

To validate the estimated losses, results were compared with values reported in the literature. For economic impacts, the expected annual losses (given that carbon emissions are directly related to energy consumption) are consistent with the empirical data reported by Ruggieri et al. [77] for multifamily residential buildings in Southern Italy and the Islands. Specifically, the observed average primary energy consumption of 138 kWh/m$^2$ corresponds to an annual cost range of 15.1-20.7 EUR/m$^2$ when using electricity and gas price data from Eurostat for the period 2000-2019 (analyzed by the authors). The estimated value falls within this range and tends toward the upper bound, reflecting the energy price higher than those observed during the reference period. For excess mortality, the estimated values were compared with those reported by García-León et al. [78]. That study projects between 28,285 and 45,683 heat-related deaths for the year 2050, which corresponds to an excess mortality rate of 0.052-0.084 per 100 persons, when normalized by the 2050 population projected by the Italian National Institute of Statistics. This range is consistent with the order of magnitude of the estimates obtained in the present study.

## 4. Discussion

### *4.1. Probabilistic framework and its applicability*

The proposed PBEE-based framework provides a probabilistic method to quantify the expected consequences of heat events. It employs Monte Carlo simulations within a modular structure, clearly separating analysis stages (hazard, building, fragility, loss). This modularity allows explicit propagation of multiple sources of uncertainty, including climate variability, building characteristics and human response. The methodology begins with hazard analysis, defining hazard curves through a selected IM. Building simulations

**Table 8**
Expected annual losses.

| Annual Loss | Historical | 2050 SSP2-4.5 | 2050 SSP3-7.0 | 2050 SSP5-8.5 | 2080 SSP2-4.5 | 2080 SSP3-7.0 | 2080 SSP5-8.5 |
|---|---|---|---|---|---|---|---|
| Economic [EUR/m$^2$] | 20.34 | 27.33 | 26.75 | 28.67 | 31.39 | 33.66 | 36.89 |
| Emission [kg $CO_2$e/m$^2$] | 24.40 | 35.76 | 35.00 | 37.49 | 41.03 | 43.98 | 48.17 |
| Excess deaths [x 100 person] | 0.003 | 0.055 | 0.051 | 0.064 | 0.074 | 0.075 | 0.079 |

generate EDPs, such as energy and thermal demand under specific heat events. Fragility curves are then derived to estimate the probability of exceeding defined response metrics, here represented as energy efficiency degradation (via EUI) and unacceptable thermal comfort levels (via SET). Monte Carlo simulations propagate uncertainties across all modules, enabling estimation of expected annual losses or other decision-relevant metrics. The framework is illustrated through a representative multi-story case study, designed to demonstrate capabilities rather than provide location-specific benchmarks. Results highlight the framework's practical utility: it can compute both probable losses for specific climate events and annualized expected losses from loss curves, with outcomes represented in risk matrices to evaluate building performance against design thresholds and various hazard return periods.

Although its flexible structure allows refinement of individual analysis modules as new data or models become available, the application of the PBEE-based framework depends on the availability and quality of input data. In the hazard module, unlike traditional assessments that rely on a limited set of representative scenarios, the probabilistic approach benefits from a larger ensemble of weather data to capture the variability of current and future conditions. While compiling multiple datasets may seem resource-intensive, it is a one-time effort that significantly enhances result accuracy. The reliability of the building analysis relies on proper characterization of uncertainties in building characteristics and operational usage, which can be informed by existing research on sensitivity analysis and uncertainty quantification [e.g. Refs [79,80] Another critical element is the definition of fragility thresholds, which may vary across countries and climate zones - for example, due to differences in human thermal adaptability in thermal fragility models. Such thresholds can also be guided by local standards and guidelines for energy-efficient buildings, as illustrated in the case study application.

Overall, the PBEE-based framework is a versatile tool for designers, planners and insurers, enabling the integration of probabilistic heat risk into operational and strategic decision-making. At the building level, it can guide design and retrofitting strategies by using loss-based matrices or direct loss-based design approaches [81] to define holistic interventions and inform technology selection aligned with specific performance objectives, allowing target loss levels (e.g. energy cost value) to be achieved from the early design stages. This approach enables designers to evaluate alternatives not only based on initial costs or local code compliance, but also on expected economic, environmental and social losses. Beyond individual buildings, the framework can support more reliable neighborhood- or district-scale planning, for example by generating heat loss curves for building archetypes providing average probable losses and associated uncertainty bounds. However, extending the framework's applicability from individual buildings to urban or regional planning requires careful consideration of transferability. This entails incorporating multiple building typologies, diverse climatic contexts and validation against additional datasets (e.g., energy consumption records, demographic data) to ensure probabilistic heat risk estimates remain robust across conditions. Such an approach also enables insurers to implement risk-based pricing, conduct portfolio analysis and integrate heat risk with other hazard models.

The proposed PBEE-based framework provides building-level probabilistic loss estimates, consistent with the catastrophe modelling interpretation of risk. While it does not directly capture societal vulnerability or governance, these estimates can still support multi-level decision-making (from individual building retrofits to broader urban planning interventions) enabling more targeted evidence-based risk management. By modelling single-property characteristics, the PBEE framework allows reliable estimation of asset-level risk, which can subsequently be aggregated to generate large-scale indicators, for example using ‘standard’ buildings or archetypes. These loss values can be incorporated into resilience assessment frameworks to quantify the response (e.g., number of deaths, hospitalization) and recovery (e.g., cooling energy cost, downtime) capacity of buildings, translating them into equivalent resilience scores, such as Resilience Readiness Levels (e.g., Ref. [82]). The framework's outputs can guide policymakers in prioritizing interventions and allocating adaptation investments based on total expected losses, and designing early warning systems or sensor placement strategies informed by uncertainty levels. The methodology is also able to integrate social dimensions of vulnerability, including advanced models in the loss module that consider human thermal adaptability and population sensitivity, alongside propagating uncertainties in behavioral responses (e.g., occupancy patterns, use of cooling systems, coping strategies). In particular, a key advantage of the methodology is its alignment with established hazard frameworks, such as seismic, wind and flood. By using a consistent structure and comparable impact metrics (e.g., cost, carbon emissions, deaths), the framework supports multi-hazard risk assessments and integration into existing vulnerability frameworks, improving communication of heat-related risks and providing insights for holistic resilience planning.

### *4.2. Limitations*

The study focuses on developing and demonstrating the methodology, using a single building typology in one city for validation, and is not intended to produce generalizable conclusions about heat resilience across broader building stocks or regions. Nonetheless, certain limitations should be considered when interpreting the case study results.

Hazard characterization relies on an IM captured through probabilistic hazard curves based on annual maxima (CDD) and employs a downscaled EPW morphing approach to incorporate climate change impacts. While this method is commonly used in practice, it may underestimate heatwave extremes, which in turn affects the absolute magnitude of the estimated losses and, consequently, the policy relevance of the numerical results. Moreover, the approach captures long-term climate variability and occurrence uncertainty, but does not explicitly represent individual heatwave episodes or adopt a specific heatwave definition, which can vary in thresholds and duration across countries and contexts.

In the building energy model, an ideal HVAC system was assumed to meet cooling demand, with electricity consumption directly proportional to the cooling load, without accounting for real-world system efficiencies or correlations with external temperature. Ventilation and infiltration were included to quantify their impact on energy costs, but indoor air quality degradation was not considered as a health outcome, and only mortality rates were modelled. Variations in grid electricity emission factors under different

climate scenarios were also not explicitly included. While the study propagates uncertainties related to hazard and consequences (e.g., costs, emissions, excess deaths), additional sources of uncertainty, such as operational usage, material properties or cooling setpoints, could also be incorporated.

The study focuses on probabilistic heat risk in terms of health and well-being, using energy efficiency and indoor thermal comfort as representative performance metrics, while physical heat-related damage to buildings was not assessed. Broader social dimensions, such as equity and lived exposure, were also not explicitly modelled. In the mortality analysis, the study assumes that health outcomes occur once the SET value exceeds a predefined unsafe threshold, and excess deaths were computed assuming no adaptive capacity across different age groups (20-85+). However, multi-factor exposure pathways (e.g., age, pre-existing health conditions, socioeconomic status) should be considered to improve this calculation, and local calibration is essential to ensure that the resulting loss functions accurately reflect the vulnerabilities of population and building stock.

### *4.3. Future work*

The modular design of the PBEE-based framework allows flexibility for future improvements. The hazard module could be replaced with higher-resolution or alternative climate projections, including datasets that better capture extreme heat events, which is particularly relevant for policy-oriented applications. The methodology could also explicitly incorporate heatwave events, for example by using Heat Wave Intensity-Duration-Frequency probabilistic curves [83] or national heatwave definitions to define exceedance probabilities, thereby refining heat exposure and vulnerability assessments for specific extreme event scenarios of interest. Future analyses could further explore defining hazard curves based on different IMs and evaluating their relevance for specific building assets, consequence quantification or problem contexts.

In building modeling, HVAC simulations could be refined to include the efficiency of cooling systems and climate scenario-dependent electricity emission factors could be incorporated to improve estimates of carbon impacts. The framework allows the integration of additional fragility curves, such as those related to heat-induced physical damage (e.g., roof deformations, cracking of façades), to estimate probable repair costs and combine them with energy costs to derive total economic losses. Indoor air quality impacts could also be included, translating reductions in ambient emissions into avoided health effects using health damage functions. This is particularly relevant because building interventions without adequate ventilation may worsen indoor air quality, potentially leading to adverse health outcomes and costs that offset the expected economic benefits.

This paper considers energy performance and thermal discomfort as representative decision variables to demonstrate the application of the framework. However, the framework can also accommodate detailed social-health profiles, population-specific vulnerabilities and behavioral responses, which could be used to refine the definition of fragility curves (e.g., threshold levels or different RM indicator) and the conversion into probable consequences in the loss module (e.g., propagating uncertainty in behavioral responses, selected consequence metrics). Incorporating broader social aspects and environmental dimensions (such as local heat-island effects or building-level microclimate conditions impacting hazard definition), the framework can provide a more comprehensive estimation of final multi-domain risk values.

In addition to further validating the approach at the building level - such as assessing thermal zoning or floor-specific risk - the methodology could be extended to different building typologies and adapted to local policy requirements, for example to define context-specific fragility thresholds (e.g. for energy efficiency degradation). Such extensions would enable scaling from individual buildings to urban or district levels, allowing the derivation of probabilistic loss curves for building archetypes. These curves could support urban intervention planning and loss-based policy decisions, as well as facilitate integrated multi-risk assessments.

## 5. Conclusions

This paper presents a probabilistic framework, grounded in Performance-Based Engineering principles, for assessing building vulnerability and risk under heat stress. The approach is structured into modular analysis components (hazard, building, fragility, loss) linked through conditional probabilities, such that each stage depends only on the outcome of the preceding one. Monte Carlo simulations are employed to propagate uncertainties across modules and quantify key decision variables, including monetary losses, operational carbon emissions and health impacts, through probabilistic loss functions. The framework's step-by-step implementation is demonstrated through application to a multi-story building, illustrating its ability to integrate climate variability and consequence uncertainty, and to evaluate their effects on expected losses. The results highlight the framework's potential to support informed retrofit and design decisions, either by using loss-based design matrices to verify performance against predefined consequence thresholds or by employing loss curves to estimate holistic annualized losses in terms of energy costs, carbon emissions and heat-related mortality. By adopting a probabilistic formulation analogous to that used for other hazards, such as earthquakes, the framework facilitates the integration of heat vulnerability into quantitative multi-hazard risk assessment processes.

The proposed approach is demonstrated using a single building typology in one city and is not intended to produce generalizable conclusions about heat risk. Nonetheless, while limitations related to the modeling assumptions in individual modules should be considered when interpreting the results, the case study demonstrates the framework's capability to consistently propagate uncertainties within a unified probabilistic framework. In particular, further development of fragility and vulnerability models that incorporate local population sensitivities would enhance the assessment, enabling more comprehensive characterization of risk to support both design and policy applications. Sensitivity analyses could also help identify the most influential parameters affecting outcomes and should be considered to improve the loss estimate robustness. Future developments will focus on refining the characterization of climate hazards and building performance through the identification of suitable Intensity Measures and Engineering

Demand Parameters. While this study focused on building-level assessments, the framework could be extended to component-level analyses (individual rooms or thermal zones) to investigate how system-level performance propagates across the building. In addition, urban-scale applications could be supported by applying and validating the framework across different building archetypes, enabling the derivation of archetype-based loss functions to inform resilience planning and holistic loss mitigation strategies.

## CRediT authorship contribution statement

**Simona Bianchi:** Writing – review & editing, Writing – original draft, Visualization, Methodology, Investigation, Funding acquisition, Formal analysis, Data curation, Conceptualization. **Jonathan Ciurlanti:** Writing – review & editing, Methodology, Investigation, Formal analysis, Conceptualization.

## Declaration of competing interest

The authors declare that they have no known competing financial interests or personal relationships that could have appeared to influence the work reported in this paper.

## Acknowledgements

This study has received funding from the Dutch Research Council (NWO) under the NWO Talent Programme Veni AES 2023 (Grant Agreement no. 21129, RECLIMATE: Resource-efficient climate-resilient buildings by multi-hazard risk modelling and resilience-oriented decision making).

## Data availability

Data will be made available on request.

## References

[1] https://www.iea.org/reports/tracking-clean-energy-progress-2023.
[2] H.W. Samuelson, A. Baniassadi, P.I. Gonzalez, Beyond energy savings: investigating the co-benefits of heat resilient architecture, Inside Energy 204 (2020), https://doi.org/10.1016/j.energy.2020.117886.
[3] J. Taylor, P. Wilkinson, M. Davies, B. Armstrong, Z. Chalabi, A. Mavrogianni, P. Symonds, E. Oikonomou, S.I. Bohnenstengel, Mapping the effects of urban heat island, housing, and age on excess heat-related mortality in London, Urban Clim. 14 (4) (2015) 517–528, https://doi.org/10.1016/j.uclim.2015.08.001.
[4] https://www.iea.org/energy-system/electricity.
[5] D. García-León, P. Masselot, M.N. Mistry, A. Gasparrini, C. Motta, L. Feyen, J.C. Ciscar, Temperature-related mortality burden and projected change in 1368 European regions: a modelling study, Lancet Public Health 9 (9) (2024) e644–e653, https://doi.org/10.1016/S2468-2667(24)00179-8.
[6] United States Department of Energy, The Nexus of Building Energy Codes and Resilience, 2024. Washington, DC.
[7] B.J. He, Green building: a comprehensive solution to urban heat, Energy Build. 271 (2022) 112306, https://doi.org/10.1016/j.enbuild.2022.112306.
[8] B.J. He, Towards the next generation of green building for urban heat island mitigation: zero UHI impact building, Sustain. Cities Soc. 50 (2019) 101647, https://doi.org/10.1016/j.scs.2019.101647.
[9] Intergovernmental Panel on Climate Change, Climate Change 2021: the Physical Science Basis, IPCC, 2021.
[10] S.S. Abolhassani, M. Mastani Joybari, M. Hosseini, Parsaee, U. Eicker, A systematic methodological framework to study climate change impacts on heating and cooling demands of buildings, J. Build. Eng. 63 (2023), https://doi.org/10.1016/j.jobe.2022.105428.
[11] J.A. Fonseca, I. Nevat, G.W. Peters, Quantifying the uncertain effects of climate change on building energy consumption across the United States, Appl. Energy 277 (2020), https://doi.org/10.1016/j.apenergy.2020.115556.
[12] S. Sun, K. Kensek, D. Noble, M. Schiler, A method of probabilistic risk assessment for energy performance and cost using building energy simulation, Energy Build. 110 (2016) 1–12, https://doi.org/10.1016/j.enbuild.2015.09.070.
[13] F. Scarpa, L.A. Tagliafico, V. Bianco, Financial and energy performance analysis of efficiency measures in residential buildings. A probabilistic approach, Inside Energy (2021) 236, https://doi.org/10.1016/j.energy.2021.121491.
[14] P. Im, R. Jackson, Y. Bae, J. Dong, B. Cui, Probabilistic reliability assessment and case studies for predicted energy savings in residential buildings, Energy Build. (2020) 209, https://doi.org/10.1016/j.enbuild.2019.109658.
[15] W. Wang, L. Zhu, J. Zhang, X. Zhu, Z. Yan, M. Cao, Evaluation of energy retrofits for existing office buildings through uncertainty and sensitivity analyses: a case study of Tianjin, China, Energy Build. (2025) 331, https://doi.org/10.1016/j.enbuild.2025.115363.
[16] M. Koniorczyk, W. Grymin, M. Zygmunt, D. Gawin, Novel stochastic approach to predict the energy demand and thermal comfort in the office buildings considering materials and human-related Gaussian uncertainties, J. Build. Eng. 42 (2021), https://doi.org/10.1016/j.jobe.2021.102831.
[17] E. Kang, H. Lee, J. Yoon, H. Cho, C. Chaichana, D. Kim, Investigating the influence of uncertainty on office building energy simulation through occupant-centric control and thermal comfort integration, Energy Build. (2024) 322, https://doi.org/10.1016/j.enbuild.2024.114741.
[18] E. Prataviera, J. Vivian, G. Lombardo, A. Zarrella, Evaluation of the impact of input uncertainty on urban building energy simulations using uncertainty and sensitivity analysis, Appl. Energy 311 (2022), https://doi.org/10.1016/j.apenergy.2022.118691.
[19] C. Wang, X. Wang, F. Causone, Y. Yang, N. Gao, Y. Ye, P. Li, X. Shi, Addressing uncertainty to achieve stability in urban building energy modeling: a comparative study of four possible approaches, Build. Environ. (2025) 267, https://doi.org/10.1016/j.buildenv.2024.112197.
[20] J. Zou, G. Zhong, L. Leon Wang, A. Katal, A. Gaur, S. Yan, M. Albettar, A. Marey, Urban heatwaves and mortality: a socioeconomic and environmental study using a novel building heat vulnerability index, Cities 169 (2026), https://doi.org/10.1016/j.cities.2025.106558.
[21] Y. Luo, X. Cheng, B.J. He, B.J. Dewancker, Identification and assessment of heat disaster risk: a comprehensive framework based on hazard, exposure, adaptation and vulnerability, Int. J. Environ. Sci. Technol. (2024), https://doi.org/10.1007/s13762-024-06195-2.
[22] S.G. Nayak, S. Shrestha, P.L. Kinney, Z. Ross, S.C. Sheridan, C.I. Pantea, W.H. Hsu, N. Muscatiello, S.A. Hwang, Development of a heat vulnerability index for New York state, Public Health 161 (2018) 127–137, https://doi.org/10.1016/j.puhe.2017.09.006.
[23] C. Lin, D.B. Crawley, M. Coudert, D. Niyogi, Z. Nagy, From comfort to survival: indoor heat vulnerability during extreme events, Build. Environ. (2025), https://doi.org/10.1016/j.buildenv.2025.114070.
[24] K. Jenkins, J. Hall, V. Glenis, et al., Probabilistic spatial risk assessment of heat impacts and adaptations for London, Clim. Change 124 (2014) 105–117, https://doi.org/10.1007/s10584-014-1105-4.

[25] R. Guo, M.H. Shamsi, M. Sharifi, D. Saelens, Exploring uncertainty in district heat demand through a probabilistic building characterization approach, Appl. Energy 377 (2025), https://doi.org/10.1016/j.apenergy.2024.124411.
[26] S. Chen, R. Xu, N.H. Wong, S. Tong, J. Wang, M. Santamouris, A probabilistic framework for predicting spatiotemporal intensity and variability of outdoor thermal comfort, Build. Environ. (2026) 289, https://doi.org/10.1016/j.buildenv.2025.114102.
[27] D.P. Jenkins, S. Patidar, P. Banfill, G. Gibson, Developing a probabilistic tool for assessing the risk of overheating in buildings for future climates, Renew. Energy 61 (2014) 7–11, https://doi.org/10.1016/j.renene.2012.04.035.
[28] A. de Angelis, F. Ascione, R.F. de Masi, M.R. Pecce, G.P. Vanoli, A novel contribution for resilient buildings, in: Theoretical Fragility Curves: Interaction Between Energy and Structural Behavior for Reinforced Concrete Buildings, vol. 10, Buildings, 2020, pp. 1–28, https://doi.org/10.3390/buildings10110194, 11.
[29] D. Szagri, Z. Szalay, Theoretical fragility curves – A novel approach to assess heat vulnerability of residential buildings, Sustain. Cities Soc. 83 (2022), https://doi.org/10.1016/j.scs.2022.103969.
[30] S. Bianchi, J. Ciurlanti, M. Overend, S. Pampanin, A probabilistic-based framework for the integrated assessment of seismic and energy economic losses of buildings, Eng. Struct. 269 (2022), https://doi.org/10.1016/j.engstruct.2022.114852.
[31] K. Kim, A. Luna-Navarro, J. Ciurlanti, S. Bianchi, A multi-criteria decision support framework for designing seismic and thermal resilient facades, Architecture, Structures and Construction 4 (2024) 195–210, https://doi.org/10.1007/s44150-024-00116-0.
[32] K.A. Porter, An overview of peer's performance-based earthquake engineering methodology. Ninth International Conference on Applications of Statistics and Probability in Civil Engineering, San Francisco, US, 2003.
[33] J. Moehle, G.G. Deierlein, A framework methodology for performance-based earthquake engineering, in: 13th World Conference on Earthquake Engineering Vancouver, B.C., Canada, 2004.
[34] S. Günay, K.M. Mosalam, PEER performance-based earthquake engineering methodology, revisited, J. Earthq. Eng. 17 (6) (2013) 829–858, https://doi.org/10.1080/13632469.2013.787377.
[35] J. Hogan, I. Almufti, M. Ackerson, Redi™: Resilience-Based Design Guidelines for Floods, 2023. Arup.
[36] M. Ciampoli, F. Petrini, G. Augusti, Performance-Based Wind Engineering: towards a general procedure, Struct. Saf. 33 (6) (2011) 367–378, https://doi.org/10.1016/j.strusafe.2011.07.001.
[37] I.J. Hall, R.R. Prairie, H.E. Anderson, E.C. Boes, Generation of a typical meteorological year. https://www.osti.gov/biblio/7013202, 1978.
[38] M. Ekström, M.R. Grose, P.H. Whetton, An appraisal of downscaling methods used in climate change research, WIREs Clim. Change 6 (2015) 301–319, https://doi.org/10.1002/wcc.339.
[39] M. Meinshausen, Z.R.J. Nicholls, J. Lewis, et al., The shared socio-economic pathway (SSP) greenhouse gas concentrations and their extensions to 2500, Geosci. Model Dev. (GMD) 13 (8) (2020) 3571–3605, https://doi.org/10.5194/gmd-13-3571-2020.
[40] T.R. Oke, City size and the urban heat island, Atmos. Environ. 7 (8) (1973) 769–779, https://doi.org/10.1016/0004-6981(73)90140-6.
[41] S. Belcher, J. Hacker, D. Powell, Constructing design weather data for future climates, Build. Serv. Eng. Res. Tecnol. 26 (1) (2005) 49–61, https://doi.org/10.1191/0143624405bt112oa.
[42] A. van Paassen, Q. Luo, Weather data generator to study climate change on buildings, Build. Serv. Eng. Res. Tecnol. 23 (4) (2002) 251–258, https://doi.org/10.1191/0143624402bt048oa.
[43] V.M. Nik, A. Sasic Kalagasidis, Impact study of the climate change on the energy performance of the building stock in Stockholm considering four climate uncertainties, Build. Environ. 60 (2013) 291–304, https://doi.org/10.1016/j.buildenv.2012.11.0.
[44] US Department of Energy's Building Technologies Office, Energyplus. DOE-BTO, 2001.
[45] W. Tian, A review of sensitivity analysis methods in building energy analysis, Renew. Sustain. Energy Rev. 20 (2013) 411–419, https://doi.org/10.1016/j.rser.2012.12.014.
[46] K. Porter, R. Kennedy, R. Bachman, Creating fragility functions for performance-based earthquake engineering, Earthq. Spectra 23 (2) (2007) 471–489, https://doi.org/10.1193/1.2720892.
[47] K.J. Collins, A.N. Exton-Smith, Thermal homeostasis in old age, J. Am. Geriatr. Soc. 31 (9) (1983) 519–524.
[48] A.L. Hass, J.D. Runkle, M.M. Sugg, The driving influences of human perception to extreme heat: a scoping review, Environ. Res. 197 (2021), https://doi.org/10.1016/j.envres.2021.111173.
[49] CDC (U.S. Centers for Disease Control and Prevention), *Indicator: Heat-Related Mortality* (Annual National Totals Provided by National Center for Environmental Health Staff in June 2024), National Center for Health Statistics, 2024 [Data set], https://ephtracking.cdc.gov.
[50] P. Masselot, M.N. Mistry, S. Rao, et al., Estimating future heat-related and cold-related mortality under climate change, demographic and adaptation scenarios in 854 European cities, Nat. Med. 31 (4) (2025) 1294–1302, https://doi.org/10.1038/s41591-024-03452-2.
[51] G.G. Deierlein, H. Krawinkler, C.A. Cornell, A framework for performance-based earthquake engineering. Pacific Conference on Earthquake Engineering, 2003.
[52] A. Ghobarah, Performance-based design in earthquake engineering: state of development, Eng. Struct. 23 (8) (2001) 878–884, https://doi.org/10.1016/S0141-0296(01)00036-0.
[53] S. Bianchi, Integrating resilience in the multi-hazard sustainable design of buildings, Disaster Prevention and Resilience 2 (2023) 14, https://doi.org/10.20517/dpr.2023.16.
[54] Housing Europe, Does One Size Fit all? Impact of Minimum Energy Performance Standards in the Revision of the Energy Performance Building Directive, Final Report, 2021.
[55] ANSI/ASHRAE 55, Thermal Environmental Conditions for Human Occupancy, American National Standard, 2023.
[56] S. Bianchi, M. Matteoni, K. Kim, et al., Resilience readiness levels for buildings: establishing multi-hazard resilience metrics and rating systems, Int. J. Disaster Risk Reduct. (2025), https://doi.org/10.1016/j.ijdrr.2025.105746.
[57] Federal Emergency Management Agency, Seismic Performance Assessment of Buildings Methodology, vol. 1, 2018. Washington DC, USA.
[58] Ufficio Rapporti con l'Unione Europea, Proposta Di Direttiva Del Parlamento Europeo E Del Consiglio Che Modifica La Direttiva 2010/31/UE Sulla Prestazione Energetica Nell'Edilizia (COM(2016)765), 2017. Rome, Italy (in Italian).
[59] T. Loga, B. Stein, N. Diefenbach, TABULA building typologies in 20 European countries—Making energy-related features of residential building stocks comparable, Energy Build. 132 (2016) 4–12, https://doi.org/10.1016/j.enbuild.2016.06.094.
[60] D.P.R., Regolamento Recante Norme per la Progettazione, L'Installazione, L'Esercizio E la Manutenzione Degli Impianti Termici Degli Edifici Ai Fini Del Contenimento Dei Consumi Di Energia, in Attuazione Dell'Art. 4, Comma 4, Della L. 9 Gennaio 1991, N. 10. Pubblicato Nella Gazz. Uff. 14 Ottobre 1993, N. 242, S.O, 1993 (in Italian).
[61] F. Salata, S. Falasca, V. Ciancio, G. Curci, P. de Wilde, Climate-change related evolution of future building cooling energy demand in a mediterranean country, Energy Build. 290 (2023), https://doi.org/10.1016/j.enbuild.2023.113112.
[62] NOAA, Integrated surface database (ISD) was, 06/03/2023 from, https://registry.opendata.aws/noaa-isd.
[63] R. McNeel, et al., Rhinoceros 3D, Version 6.0. Robert Mcneel & Associates, 2010. Seattle, WA.
[64] T. Lhendup, S. Lhundup, Comparison of methodologies for generating a typical meteorological year (TMY), Energy Sustain. Dev. 11 (3) (2007) 5–10, https://doi.org/10.1016/S0973-0826(08)60571-2.
[65] E. Rodrigues, M.S. Fernandes, D. Carvalho, Future weather generator for building performance research: an open-source morphing tool and an application, Build. Environ. (2023) 233, https://doi.org/10.1016/j.buildenv.2023.110104.
[66] IPCC, Introduction to WGII AR6 Fact Sheets, Sixth Assessment Report, Intergovernmental Panel on Climate Change, 2023.
[67] ASHRAE, Standard 169-2021, Climatic Data for Building Design Standards, 2021.
[68] Ministero delle Infrastrutture, Aggiornamento delle Norme Tecniche per le Costruzioni, Supplemento Ordinario N 8 Alle G.U. No 42 Del 20/02/2018, 2018. Rome, Italy (in Italian).
[69] A. Machard, P. Salvati, M. Tootkaboni, et al., Typical and extreme weather datasets for studying the resilience of buildings to climate change and heatwaves, Sci. Data 11 (2024) 531, https://doi.org/10.1038/s41597-024-03319-8.

[70] G.B. Anderson, M.L. Bell, R.D. Peng, Methods to calculate the heat index as an exposure metric in environmental health research, Environ. Health Perspect. 121 (2013) 10. https://doi.org/10.1289/ehp.1206273.
[71] https://www.weather.gov/ffc/hichart.
[72] F. Jalayer, R. De Risi, G. Manfredi, Bayesian Cloud Analysis: efficient structural fragility assessment using linear regression, Bull. Earthq. Eng. 13 (2015) 1183–1203, https://doi.org/10.1007/s10518-014-9692-z.
[73] K. Kim, S. Bianchi, T. Konstantinou, M. Overend, J. Ciurlanti, A. Luna-Navarro, Thermal resilience to extreme heat: Preliminary Study on thermal fragility curves, in: U. Berardi (Ed.), Multiphysics and Multiscale Building Physics. IABP 2024. Lecture Notes in Civil Engineering, Springer, Singapore, 2025, https://doi.org/10.1007/978-981-97-8309-0_47.
[74] G.M. Calvi, L. Sousa, C. Ruggeri, Energy efficiency and seismic resilience: a common approach. Multi-Hazard Approaches to Civil Infrastructure Engineering, Springer Intern, 2016, p. 9. https://link.springer.com/chapter/10.1007/978-3-319-29713-2_9.
[75] J. Wenjie, et al., Interpretation of standard effective temperature (SET) and explorations on its modification and development, Build. Environ. 210 (2022), https://doi.org/10.1016/j.buildenv.2021.108714.
[76] P. Balcombe, N.P. Brandon, A.D. Hawkes, Characterising the distribution of methane and carbon dioxide emissions from the natural gas supply chain, J. Clean. Prod. 172 (2018) 2019–2032, https://doi.org/10.1016/j.jclepro.2017.11.223.
[77] G. Ruggieri, F. Andreolli, P. Zangheri, A Policy roadmap for the energy renovation of the residential and educational building stock in Italy, Energies 16 (2023) 1319, https://doi.org/10.3390/en16031319.
[78] D. García-León, P. Masselot, M. N Mistry, A. Gasparrini, C. Motta, L. Feyen, J.C. Ciscar, Temperature-related mortality burden and projected change in 1368 European regions: a modelling study, Lancet Public Health 9 (9) (2024) e644–e653.
[79] V. Corrado, H.E. Mechri, Uncertainty and sensitivity analysis for building energy rating, J. Build. Phys. 33 (2) (2009) 125–156, https://doi.org/10.1177/1744259109104884.
[80] C.J. Hopfe, J.L.M. Hensen, Uncertainty analysis in building performance simulation for design support, Energy Build. 43 (10) (2011) 2798–2805, https://doi.org/10.1016/j.enbuild.2011.06.034.
[81] R. Gentile, G.M. Calvi, Direct loss-based seismic design of reinforced concrete frame and wall structures, Earthq. Eng. Struct. Dynam. 52 (14) (2023) 4395–4415, https://doi.org/10.1002/eqe.3955.
[82] S. Bianchi, et al., Resilience readiness levels for buildings: establishing multi-hazard resilience metrics and rating systems, Int. J. Disaster Risk Reduct. 128 (2025), https://doi.org/10.1016/j.ijdrr.2025.105746.
[83] O. Mazdiyasni, M. Sadegh, F. Chiang, et al., Heat wave intensity duration frequency curve: a multivariate approach for hazard and attribution analysis, Sci. Rep. 9 (2019), https://doi.org/10.1038/s41598-019-50643-w.